Posterior subthalamic nucleus (PSTh) mediates innate fear-associated hypothermia

Can Liu
National Institute of Biological Sciences, Beijing
Chia-Ying Lee
University of Tsukuba
Greg Asher
International Institute for Integrative Sleep Medicine (WPI-IIIS), University of Tsukuba
Liqin Cao
International Institute for Integrative Sleep Medicine (WPI-IIIS), University of Tsukuba
Yuka Terakoshi
International Institute for Integrative Sleep Medicine (WPI-IIIS), University of Tsukuba, Tsukuba
Peng Cao
National Institute of Biological Sciences, Beijing https://orcid.org/0000-0001-7739-6857
Reiko Kobayakawa
Kansai Medical University
Ko Kobayakawa
Kansai Medical University
Katsuyasu Sakurai
International Institute for Integrative Sleep Medicine (WPI-IIIS), University of Tsukuba
Qinghua Liu (liuqinghua@nibs.ac.cn)
National Institute of Biological Sciences, Beijing

Article

Keywords: 2-methyl-2-thiazoline (2MT), innate fear, hypothermia, posterior subthalamic nucleus (PSTh), external lateral parabrachial subnucleus (PBel), nucleus of the solitary tract (NTS)

Posted Date: December 2nd, 2020

DOI: https://doi.org/10.21203/rs.3.rs-112564/v1

Posterior subthalamic nucleus (PSTh) mediates innate fear-associated hypothermia

Can Liu[1,2,3], Chia-Ying Lee[4], Greg Asher[4], Liqin Cao[4], Yuka Terakoshi[4], Peng Cao[2,3], Reiko Kobayakawa[5], Ko Kobayakawa[5], Katsuyasu Sakurai[4*] & Qinghua Liu[2,3,4*]

[1]Peking University–Tsinghua University–NIBS Joint Graduate Program, School of Life Sciences, Tsinghua University, Beijing, China; [2]National Institute of Biological Sciences (NIBS), Beijing 102206, China; [3]Tsinghua Institute of Multidisciplinary Biomedical Research (TIMBR), Tsinghua University, Beijing 102206, China; [4]International Institute for Integrative Sleep Medicine (WPI-IIIS), University of Tsukuba, Tsukuba, Ibaraki 305-8575, Japan; [5]Functional Neuroscience Lab, Kansai Medical University, Hirakata, Osaka 573-1010, Japan.

* Corresponding authors:

sakurai.katsuyasu.gm@u.tsukuba.ac.jp

liuqinghua@nibs.ac.cn

Key words: 2-methyl-2-thiazoline (2MT), innate fear, hypothermia, posterior subthalamic nucleus (PSTh), external lateral parabrachial subnucleus (PBel), nucleus of the solitary tract (NTS)

ABSTRACT

Mammals normally maintain a constant body temperature irrespective of their environmental temperature. However, emotions such as fear can trigger acute changes in body temperature accompanying defensive behaviors to enhance survival in life-threatening conditions. The neural mechanisms of fear-associated thermoregulation remain unclear. Here, we find that innate fear odor 2-methyl-2-thiazoline (2MT) evokes rapid hypothermia and elevated tail temperature, indicative of vasodilation-induced heat dissipation, in wild-type mice, but not in mice lacking Trpa1, the chemosensor for 2MT. Following 2MT exposure, wild-type but not *Trpa1*$^{-/-}$ mice exhibit high c-fos expression in the posterior subthalamic nucleus (PSTh), external lateral parabrachial subnucleus (PBel), and nucleus of the solitary tract (NTS). Tetanus toxin light chain (TeLC)-mediated inactivation of NTS-projecting PSTh neurons blunts 2MT-evoked hypothermia and abrogated tail temperature increase. Optogenetic activation of the PSTh-rostral NTS (RNTS) pathway specifically induces hypothermia and elevated tail temperature. Moreover, selective opto-stimulation of 2MT-activated PSTh-projecting PBel neurons, by capturing activated neuronal ensembles (CANE), induces hypothermia and elevated tail temperature. Conversely, chemogenetic suppression of vGlut2^{+} neurons in PBel and PSTh or PSTh-projecting PBel neurons attenuates 2MT-evoked hypothermia and tail temperature increment. Taken together, these results uncover a novel PBel-PSTh-NTS neural pathway that underlies 2MT-evoked innate fear-associated hypothermia and tail vasodilation.

INTRODUCTION

The regulation of body temperature–thermoregulation–is essential to life. While ectothermic (cold-blooded) animals, such as reptiles, take on the temperature of their environment, endothermic (warm-blooded) animals, such as mammals, maintain their body temperature in a very narrow range regardless of the ambient temperature[1-7]. In mammals, the body temperature can also be temporally up- or down-regulated to promote survival in response to specific environmental and physiological challenges[8-10]. For instance, fever is a common physiological response activated by the immune system to combat infections[11,12]. Some animals undergo hibernation or torpor, which are physiologically inactive states characterized by hypothermia and hypometabolism, to conserve energy and survive when temperature or food source is low[13-16].

The body temperature can also be regulated by emotions, such as fear and anger. Fear elicits a series of stereotypical defensive behaviors and physiological responses to enhance animal survival[17]. For example, freezing is a typical defensive behavior in preys to avoid detection by predators[18-20]. Autonomic activities, such as body temperature, heart rate, and blood pressure, can all be regulated as part of the "fight or flight" response under learned and innate fear conditions[21,22]. Depending on the type of external stimuli and animal's internal state, these physiological responses can be quite variable, including hyperthermia or hypothermia, tachycardia or bradycardia, and hypertension or hypotension[17,23,24]. Learned fear, whereby animals are trained by presenting various sensory cues paired with foot shocks, causes elevated core body temperature accompanied by decreased skin temperature in tail and paw[25]. It has also been reported that innate fear stimuli, such

as ferret or fox odor, induces hyperthermia in rats[26,27]. On the other hand, long-term restraint/immobilization, hypoxia or inescapable stress have been shown to evoke hypothermia in mammals[28-30]. In humans, fear or anxiety has a similar effect on body temperature changes and vasoconstriction/vasodilation, creating rapid chills or hot sensation[31,32]. The term “spine chilling” is frequently used to describe extreme fear in many languages. However, the neural mechanisms that underlie various fear-associated rapid changes in body temperature remain largely unknown.

It has been shown that 2-methyl-2-thiazoline (2MT), a potent analog of predator odor 2,4,5-trimethyl-3-thiazoline (TMT), elicits highly robust innate fear/defensive behaviors, such as freezing, in naïve mice[33,34]. Through forward genetics screening of randomly mutagenized mice, we identified the transient receptor potential A1 (*Trpa1*) mutant as deficient for 2MT/TMT- and snake skin-evoked innate defensive behaviors[33]. Furthermore, we demonstrated that Trpa1, a well-known receptor for pungent/irritant chemicals, functions as a novel chemosensor for 2MT/TMT, and that Trpa1-mediated nociception in trigeminal ganglion (TG) neurons contribute critically to 2MT-induced innate freezing[33]. In this study, we investigated the neural mechanisms of 2MT-evoked innate fear-associated thermoregulation. We found that exposure to 2MT could evoke rapid hypothermia accompanied by elevated tail temperature in wild-type mice, but not in *Trpa1*$^{-/-}$ mice. Our results indicate that the posterior subthalamic nucleus (PSTh) functions as a critical hub that connects the external lateral parabrachial subnucleus (PBel) to the nucleus of the solitary tract (NTS) to mediate 2MT-evoked innate fear-associated hypothermia and tail vasodilation.

RESULTS

We compared the 2MT-induced thermoregulatory response between wild-type and *Trpa1*$^{-/-}$ mice using a behavior paradigm as previously described[33,35]. To study the effect of 2MT on the change of body temperature, we used infrared (IR) thermography combined with implanted telemetry transmitter to measure in real time the cutaneous and core body temperature, respectively (Fig. 1a). Although skin temperature normally reflects core body temperature[36], IR thermography allows us to simultaneously measure the temperature of a large body surface, including the tail and trunk areas[37]. Moreover, IR imaging of body surface is useful to detect additional thermoregulatory alterations, such as vasodilation-induced heat dissipation.

In the absence of fear odor, both the skin temperature (Ts), defined by the highest temperature in the back, and the core body temperature (Tc) remained stable (Fig. 1c-1f). Upon 2MT exposure in wild-type mice, both the skin and core body temperature began to decrease immediately in wild-type mice (Fig. 1c and 1e), with the lowest temperature reached at approximately 10 min after 2MT exposure (Fig. 1c and 1e, maximal ΔTs=-4.02±0.38°C; maximal ΔTc=-2.73±0.18°C;). The average ΔTs and ΔTc was -2.78±0.26°C and -2.10±0.10℃, respectively, during 2MT exposure (Fig. 1d and 1f). Interestingly, we also observed a transient sharp increase in the tail temperature (maximal ΔTt=6.78±0.08°C; average ΔTt=2.29±0.28°C) of wild-type mice after 2MT exposure (Fig.1b, arrow, 1g, 1h), which preceded the lowest point of body temperature (Fig.1c, 1e and 1g). Because mouse tail plays a crucial role in vasodilation-induced heat dissipation[38], these observations suggest that heat dissipation over the tail surface contributes critically to 2MT-evoked

hypothermia. By contrast, we observed no significant changes in the tail, skin, or core body temperature (maximal ΔTt=0.52±0.10°C; maximum ΔTs= -0.54±0.05 °C; maximum ΔTc=-0.31±0.07 °C) in *Trpa1*$^{-/-}$ mice following 2MT treatment (Fig.1b-1h). Moreover, we found that exposure to cinnamaldehyde, a well-known Trpa1 agonist, did not induce hypothermia in wild-type mice (Supplementary Fig. 1a and 1b). Taken together, these results indicate that innate fear odor 2MT induces rapid hypothermia and elevated tail temperature in wild-type mice, which are both abolished in mice deficient for Trpa1, the chemosensor for 2MT.

Comparative analysis of 2MT-induced c-fos expression in wild-type and *Trpa1*$^{-/-}$ mice

To investigate the neural mechanism responsible for 2MT-induced hypothermia, we performed immunohistochemistry to compare the expression of immediate early gene *c-fos* in many brain regions of wild-type and *Trpa1*$^{-/-}$ mice following 2MT exposure (Fig. 1i and 1j and Supplementary Fig. 1c-1l). Consistently, we observed that *Trpa1*$^{-/-}$ mouse brains exhibited diminished c-fos expression relative to wild-type mouse brains in several known fear/stress, thermoregulation and vasodilation/vasoconstriction centers, such as the central amygdala (CeA), paraventricular hypothalamic nucleus (PVN) and ventrolateral periaqueductal gray (vlPAG), as well as PSTh, PBel, NTS and caudal ventrolateral medulla (CVML) (Fig. 1i and 1j and Supplementary Fig. 1c-1e and 1l)[4,20,39-45]. Conversely, we found significantly more c-fos expressing neurons in the median preoptic nucleus (MnPO), ventromedial preoptic nucleus (VMPO) and rostral ventrolateral medulla (RVML) in *Trpa1*$^{-/-}$ mice relative to wild-type mice (Supplementary Fig.1g, 1h and 1k).

Because neurons that are inhibited during 2MT response will not be c-fos-positive, this result suggests a possibility that some unknown neural pathway may contribute to 2MT-evoked hypothermia through suppression of MnPO/VMPO neurons. We did not observe significant difference in c-fos expression in the dorsolateral periaqueductal gray (dlPAG), dorsal part of the lateral parabrachial nucleus (LPBD), and rostral raphe pallidus nucleus (rRpa) (Supplementary Fig. 1f, 1i and 1j). These observations suggest that the thermoregulatory center LPBD and vasomotor control center rRpa are unlikely to play a critical role in 2MT-evoked hypothermia and tail vasodilation (see detailed discussion on the vasomotor control centers, rRpa, CVML and RVML, in the Discussion).

It is well-known that cutaneous warm and cold sensory signals are conveyed from the lateral parabrachial nucleus (LPB) to the preoptic area (POA) by two distinct glutamatergic pathways, the LPBD and LPBel. PBel contains a functionally heterogeneous neural population involved in the processing of diverse sensory information, such as temperature, taste, and pain[1-3,50-56]. NTS is the crucial relay nucleus for many thermoregulation-related signal transmission[4,40-42]. For example, adenosine A1 receptor activation in NTS induces hypothermia[40]. Additionally, NTS activity is involved in the brown adipose tissue-dependent thermoregulation[4,41,42]. PSTh is well recognized as a motor controlling center[57], of which deep brain stimulation is employed to treat Parkinson's disease[58,59]. However, PSTh has not previously been implicated in thermoregulation. Based on the comparative c-fos analysis of wild-type and *Trpa1*$^{-/-}$ mouse brains following 2MT exposure, we hypothesized that the PBel, NTS, and PSTh may be directly involved in 2MT-evoked hypothermia.

NTS neurons receive synaptic inputs from PSTh neurons

A major autonomic response to reduce body temperature is through the vasodilation-induced heat dissipation in the glabrous organs, such as the mouse tail[3]. Accordingly, we observed that 2MT exposure elicited an acute elevation of tail temperature, indicative of vasodilation-induced heat dissipation, prior to reaching the lowest point of body temperature (Fig.1b-1h). It has been reported that NTS activation may induce tail vasodilation through inhibition of neural activity in the rostral ventrolateral medulla (RVLM), a pivotal vasomotor control nucleus in the brain stem[43]. Thus, we hypothesized that the upstream input nuclei of NTS could play an important role in 2MT-induced hypothermia and elevated tail temperature.

To identify the upstream nuclei that project to NTS, we performed retrograde tracing of NTS neurons by unilateral injection of cholera toxin B subunit (CTB)-conjugated Alexa Fluor 488 (CTB-488) into the NTS (Fig. 2a and Supplementary Fig. 2a). CTB-injected mice were exposed to 2MT to visualize 2MT-activated c-fos-expressing neurons by immunohistochemistry. In the NTS-projecting nuclei involved in 2MT-evoked hypothermia, we expected that the CTB-488 labeled neurons would show significant overlap with 2MT-activated c-fos-labeled neurons. Accordingly, we observed CTB-positive neurons in the PSTh, PBel, CeA, and PVN (Fig. 2b and Supplementary Fig. 2b-2d). Among these, PSTh exhibited the highest density of CTB-positive neurons and the highest percentage (~32%) of c-fos$^+$, CTB$^+$ double positive neurons (Fig. 2b and Supplementary Fig. 2e-2g), implicating a potential involvement of the PSTh-NTS pathway in 2MT-evoked hypothermia response.

vGlut2$^+$ PSTh neurons are critical for 2MT-evoked hypothermia and tail vasodilation

To determine the neurotransmitter type of 2MT-activated neurons in PSTh, we performed two-color fluorescence in situ hybridization using antisense RNA probes for *c-fos* and vesicular glutamate transporter 2 (*vGlut2*) or vesicular GABA transporter (*vGAT*). Our results indicated that the majority of 2MT-activated *c-fos*-positive PSTh neurons expressed *vGlut2* (87±2%), whereas a minority were *vGAT*-positive (3±1%) (Fig. 2c). Thus, the majority of 2MT-activated PSTh neurons are vGlut2-expressing excitatory neurons.

To examine whether vGlut2$^+$ PSTh neurons were critical for 2MT-evoked hypothermia, we utilized the Designer Receptors Exclusively Activated by Designer Drugs (DREADDs) system for specific suppression of vGlut2$^+$ PSTh neurons. We bilaterally injected AAV2/9-hSyn-DIO-hM4Di-mCherry or AAV2/10-EF1a-DIO-mCherry into the PSTh of *vGlut2-IRES-Cre* mice to specifically express hM4Di or mCherry in vGlut2$^+$ PSTh neurons (Fig. 2d and 2e). To suppress the neural activity of vGlut2$^+$ PSTh neurons, clozapine analog compound 21 (C21, 1mg/kg) was intraperitoneally (i.p.) administered in the mCherry- or hM4Di-expressing mice 30 min before 2MT exposure. Chemogenetic inhibition of vGlut2$^+$ PSTh neurons significantly blunted the 2MT-evoked hypothermia and tail temperature increment in hM4Di-expressing mice compared to mCherry-expressing mice (average ΔTt: hM4Di, 1.09 ± 0.14 °C vs. mCherry, 2.47 ± 0.38 °C, p=0.0097; average ΔTs: hM4Di, -1.37 ± 0.12 °C vs. mCherry, -2.14 ± 0.16 °C, p=0.0027; average ΔTc: hM4Di, -1.44±0.12 °C vs.

mCherry, -2.29±0.24 °C; p=0.0061) (Fig. 2f-2l). These results suggest that the activity of vGlut2$^+$ PSTh neurons plays a critical role in mediating 2MT-evoked hypothermia in mice.

TeLC-mediated inhibition of the NTS-projecting PSTh neurons diminished 2MT-evoked hypothermia and tail vasodilation

To determine whether the PSTh-NTS pathway was critical for 2MT-evoked hypothermia, we specifically express the tetanus toxin light chain (TeLC) in the NTS-projecting PSTh neurons through bilateral injections of AAV2/retro-hSyn-Cre expressing retrogradely transported Cre recombinase into the NTS, and AAV2/9-hSyn-FLEX-TeLC-P2A-GFP expressing Cre-dependent TeLC into the PSTh, respectively (Fig. 3a and 3b). For control mice, AAV2/9-hSyn-DIO-EGFP expressing Cre-dependent EGFP was bilaterally injected instead into the PSTh to label the NTS-projecting PSTh neurons. We found that TeLC-mediated silencing of neurotransmission in NTS-projecting PSTh neurons abrogated 2MT-evoked tail temperature increase (Fig. 3c-3e, average ΔTt: TeLC, 0.34±0.11 °C vs. EGFP, 1.40±0.17 °C, p=0.0091) and blunted 2MT-evoked hypothermia (Fig. 3f-3i, average ΔTs: TeLC, -1.12±0.12 °C vs. EGFP, -1.83±0.13 °C, p = 0.0210; average ΔTc: TeLC, -0.97±0.21 °C vs. EGFP, -2.00±0.18 °C, p=0.0214). Moreover, we observed an excellent positive correlation between the virus transduction rate and the suppression effect of 2MT-evoked hypothermia： the higher the number of TeLC-labeled NTS-projecting PSTh neurons, the lesser the reduction in the skin and core body temperature following 2MT treatment (Supplementary Fig. 3a

and 3b). These results suggest that 2MT exposure activates the PSTh-NTS pathway to induce hypothermia and tail temperature increment in mice.

Opto-stimulation of PSTh-RNTS pathway causes hypothermia and tail vasodilation

To test whether activation of the PSTh-NTS pathway could induce hypothermia, we specifically labelled the NTS-projecting PSTh neurons by bilateral injection of AAV2/retro-hSyn-ChR2-EYFP or AAV2/retro-hSyn-EGFP into the NTS for retrograde expression of Channelrhodopsin 2 (ChR2) or EGFP, respectively, and by implanting optical fibers above the PSTh (Fig.4a and 4b). Blue light stimulation of the NTS-projecting PSTh neurons resulted in hypothermia accompanied by elevated tail temperature in the ChR2-expressing mice (Fig. 4c). Quantitative analysis indicated that activation of NTS-projecting PSTh neurons triggered a significant surge in the tail temperature (average ΔTt: ChR2, 3.96±0.39 °C vs. EGFP, -0.03±0.05 °C; p<0.0001), as well as reduction in the skin and core body temperature (average ΔTs: ChR2, -1.92±0.23 °C vs. EGFP, -0.35±0.05 °C, p<0.0001; average ΔTc: ChR2, -1.81±0.21 °C vs. EGFP, -0.31±0.06 °C, p<0.0001) in ChR2-expressing mice, but not in EGFP-expressing control mice (Fig. 4d-4i). It should be noted that a potential caveat of this experiment was that retrograde-labeled PSTh neurons could project to other brain areas besides NTS that might also be involved in thermoregulation.

To further confirm whether the PSTh-NTS pathway was involved in thermoregulation, we specifically labelled vGluT2$^+$ PSTh neurons by bilateral injection of AAV2/9-EF1a-DIO-ChR2-mCherry or AAV2/9-EF1a-DIO-mCherry into the PSTh of *vGlut2-IRES-Cre* mice for expression of

ChR2 or mCherry, and implanted optical fibers on the NTS (Fig.5a). Because NTS is a rather large area, we implanted optic fibers above either the rostral (RNTS; AP coordinate -7.0) or caudal (CNTS; AP coordinate -7.8) side of NTS to distinguish which part of NTS was responsible for 2MT-induced hypothermia and tail temperature increase (Fig. 5a and 5b). Blue light stimulation of the axon terminals of PSTh neurons in RNTS resulted in robust hypothermia accompanied by elevated tail temperature in the ChR2-expressing mice, but not in mCherry-expressing mice (average ΔTt: ChR2, 4.17±0.62 °C vs. mCherry, 0.03±0.26 °C; p=0.0034; average ΔTs: ChR2, -2.39±0.16 °C vs. mCherry, -0.78±0.10 °C, p=0.0012; average ΔTc: ChR2, -1.73±0.25 °C vs. mCherry, -0.26±0.34 °C, p=0.0308) (Fig. 5c-5j and Supplementary Fig. 4). By contrast, optogenetic stimulation of CNTS-projecting PSTh neurons showed no statistically significant change in either tail temperature or skin/core body temperature relative to the control mCherry-expressing mice (average ΔTt: ChR2, 2.05±1.02 °C vs. mCherry, 0.06±0.12 °C; p=0.2248; average ΔTs: ChR2, -1.35±0.17 °C vs. mCherry, -0.87±0.10 °C, p=0.6652; average ΔTc: ChR2, -0.30±0.09 °C vs. mCherry, -0.05±0.06 °C, p=0.1067) (Fig. 5c-5j and Supplementary Fig. 4). These results suggest that the PSTh-RNTS pathway plays a critical role in mediating 2MT-evoked hypothermia in mice.

PSTh neurons receive synaptic inputs from PBel neurons

To study how 2MT activated PSTh neurons to induce hypothermia, we performed retrograde tracing to find upstream input nuclei of PSTh neurons by unilateral injection of CTB-488 into the PSTh (Fig. 6a and Supplementary Fig. 5a). CTB-488 injected mice were exposed to 2MT

to identify the CTB^+, $c\text{-}fos^+$ double positive neurons, which indicated the PSTh-projecting neurons that were also activated by 2MT exposure. While many CTB^+ neurons were found in the PBel, NTS, PVN and CeA, the PBel showed the highest density of CTB^+ neurons and highest percentage of $c\text{-}fos^+$, CTB^+ double positive neurons (Fig. 6b and Supplementary Fig. 5b-5g). Consistent with a recent report[45], our results suggest that PSTh neurons receive synaptic input from PBel neurons.

Opto-stimulation of 2MT-activated, PSTh-projecting PBel neurons causes hypothermia

If the PSTh-projecting PBel neurons are causally linked to 2MT-evoked hypothermia, then specific activation of these neurons may be sufficient to induce similar phenotypes to that caused by 2MT exposure. To test this possibility, we used the Capturing Activated Neuronal Ensembles (CANE) system to selectively label and manipulate the neurons expressing c-fos in response to 2MT exposure[53,60,61]. Briefly, singly housed Fos^{TVA} male mice were exposed to 2MT to induce transient c-fos and TVA expression in PBel neurons. After one hour, 2MT-treated mice were bilaterally injected in the PBel with AAV2/9-EF1a-DIO-ChR2-mCherry and CANE-Lv-Cre, a pseudotyped lentivirus that could specifically infect the TVA-expressing PBel neurons and express Cre recombinase (Fig. 6c and 6d). Thus, the use of CANE system restricted the expression of ChR2 to only 2MT-activated PBel neurons. In control mice, 2MT-activated PBel neurons were selectively labeled with mCherry by bilateral injection of AAV2/10-EF1a-DIO-mCherry and CANE-Lv-Cre in the PBel following 2MT exposure (Fig. 6c).

Next, we implanted optic fibers above the virus-injected PBel region for optogenetic stimulation of the cell bodies of 2MT-activated PBel neurons (Fig. 6c and 6d). We observed a significant reduction in the skin and core body temperature (average ΔTs: ChR2, -1.20±0.21 °C vs. mCherry, -0.40±0.14 °C; p=0.0147; average ΔTc: ChR2 -1.16±0.18 °C vs. mCherry, -0.13±0.20 °C; p=0.0054), accompanied by a transient increase of the tail temperature (average ΔTt: ChR2, 1.39±0.40 °C vs. mCherry, 0.14±0.04 °C; p=0.0296) in the ChR2-expressing, but not mCherry-expressing, Fos^{TVA} mice during blue light stimulation (Fig. 6e-6k). These results indicate that selective stimulation of 2MT-activated PBel neurons effectively caused hypothermic response similar to that caused by 2MT exposure in mice.

Consistent with the retrograde tracing results of PSTh neurons (Fig. 6a and 6b), we found that the axonal projections of 2MT-activated PBel neurons terminated in the PSTh (Fig. 6m). To test whether the PBel-PSTh pathway was involved in thermoregulation, we implanted optic fibers above the PSTh and stimulated the axon terminals of 2MT-activated PBel neurons by blue light (Fig. 6l and 6m). Optogenetic stimulation of the axon terminals in PSTh induced a significant reduction in the skin and core body temperature (average ΔTs: ChR2, -1.07±0.20 °C vs. mCherry, -0.29±0.15 °C, p=0.0231; average ΔTc: ChR2, -1.28±0.18 °C vs. mCherry, -0.01±0.21 °C, p=0.0017) in ChR2-expressing mice, but not in mCherry-expressing mice (Fig. 6n-6q). However, we did not observe a significant change in the tail temperature in all of the mice during blue light stimulation (data not shown), which was probably due to relatively low efficiency of neuron labeling by CANE and/or inability to activate sufficient number of PBel-PSTh axonal terminals.

An alternative explanation is that the 2MT-activated PBel neurons may also send projections to other thermoregulatory regions to induce the hypothermic responses. It has been reported that a group of PBel neurons respond to cold temperature and project to the preoptic area (POA)–a well-known thermoregulatory center[46-48,54-56]. However, we found that 2MT-activated PBel neurons did not project to the POA (Supplementary Fig. 6a), suggesting that they represent a separate neural population from those responding to cold temperature and project to POA.

Interestingly, we observed that the CANE-labled PBel neurons also projected to the CeA, a well-known region associated with fear responses (Supplementary Fig. 6b). Thus, we optogentically stimulated the axon terminals of 2MT-activated PBel neurons in the CeA by blue light, which resulted in a modest reduction in skin and core body temperature (Supplementary Fig. 6c-6g, average ΔTs: ChR2, -0.87±0.15 °C vs. mCherry, -0.31±0.04 °C, p=0.0577; average ΔTc: ChR2, -0.68±0.12 °C vs. mCherry, -0.17±0.11 °C, p=0.0320), but no change in the tail temperature (data not shown). Thus, in addition to PSTh, other brain areas downstream of PBel neurons, such as CeA, may also contribute to 2MT-induced hypothermic responses.

The PBel-PSTh pathway is critical for 2MT-evoked hypothermia and tail vasodilation

To test whether the activity of PBel neurons was involved in 2MT-evoked hypothermia and tail temperature increase, we carried out cell type-specific DREADDs inhibition experiment. First, we showed by two color in situ hybridization that the majority (~86%) of 2MT-activated PBel neurons are vGlut2-expressing excitatory neurons (Supplementary Fig. 7a). Secondly, we bilaterally injected

AAV2/9-hSyn-DIO-hM4Di-mCherry or AAV2/10-EF1a-DIO-mCherry into the PBel of *vGlut2-IRES-Cre* mice to specifically express hM4Di or mCherry in the vGlut2^{+} PBel neurons (Supplementary Fig. 7b and 7c). Administration of C21 blunted 2MT-induced tail temperature increase (average ΔTt: hM4Di, 0.56±0.26 °C vs. mCherry, 1.71±0.23 °C, p=0.0130) in the hM4Di-expressing mice relative to mCherry-expressing mice (Supplementary Fig. 7d-7f). Additionally, chemogenetic suppression of vGlut2^{+} PBel neurons also slightly attenuated 2MT-evoked hypothermia (average ΔTs: hM4Di, -1.39±0.14 °C vs. mCherry, -1.77±0.08 °C, p = 0.0370; average ΔTc: hM4Di, -1.37±0.11 °C vs. mCherry, -1.78±0.08 °C, p=0.0139) (Supplementary fig. 7d and 7g-7j). Because PBel contains highly heterogeneous populations of neurons, including neurons activated by warm or cool body temperature[54-56], the mild results in this experiment are likely due to activating different neurons of opposing functions.

To further confirm whether the PBel-PSTh pathway was critical for 2MT-evoked hypothermia, we specifically silenced the neurotransmission in the PSTh-projecting PBel neurons by inhibitory DREADDs. Briefly, the PSTh-projecting PBel neurons were labeled by bilateral injections of AAV2/retro-hSyn-Cre into the PSTh and AAV2/9-hSyn-DIO-hM4Di-mCherry or AAV2/9-hSyn-DIO-mCherry into the PBel, respectively (Fig. 7a and 7b). C21 treatment significantly blunted 2MT-induced tail temperature increase (average ΔTt: hM4Di, -0.11±0.25 °C vs. mCherry, 1.61±0.25 °C, p=0.0007) in the hM4Di-expressing mice relative to mCherry-expressing mice (Fig. 7c-7e). Moreover, chemogenetic suppression of the PSTh-projecting PBel neurons also significantly attenuated 2MT-evoked hypothermia (average ΔTs: hM4Di, -1.28±0.20 °C vs. mCherry, -

2.26±0.26 °C, p=0.0148; average ΔTc: hM4Di, -1.00±0.11 °C vs. mCherry, -1.83±0.31 °C, p=0.0250) (Fig. 7c and 7f-7i). Taken together, these results strongly suggest that 2MT-activated PBel neurons project to PSTh to mediate 2MT-evoked hypothermia and tail vasodilation.

DISCUSSION

Emotions such as fear can trigger a rapid shift in thermoregulation as part of the "fight or flight" response to dangerous situations. However, the neural mechanisms of fear-related thermoregulation remain largely unexplored. In this study, we discovered that exposure to 2MT could induce rapid hypothermia accompanied by elevated tail temperature in wild-type mice, but not in *Trpa1*$^{-/-}$ mice. Based on our current studies (this paper and Kobayakawa's co-submitted paper)[35,62], we propose a working model for the neural mechanism underlying 2MT-evoked hypothermia (Fig. 8). Innate fear odor 2MT is sensed by the nociceptive receptor Trpa1, which is expressed on the surface of the trigeminal ganglion (TG) neurons and vagal ganglion (VG) neurons. Whereas VG neurons transmit the signal to NTS[63], TG neurons transmit the signal to PB and the spinal trigeminal nucleus (Sp5) in the brainstem[64,65]. Because Sp5 neurons also project to PB[66,67], we believe that a subpopulation of vGlut2^{+} PBel neurons receive the 2MT-evoked innate fear signal directly from TG or indirectly *via* Sp5 neurons. Once activated, these vGlut2^{+} PBel neurons transmit the signal to vGlut2^{+} PSTh neurons, which then relay the signal to NTS neurons to trigger hypothermia and tail vasodilation.

In support of this model, optogenetic activation of the axon terminals or cell bodies of the NTS-projecting PSTh neurons or 2MT-activated PSTh-projecting PBel neurons effectively induces hypothermia and elevated tail temperature. Conversely, chemogenetic suppression of the vGlut2$^+$ excitatory neurons in the PBel or PSTh, or the PSTh-projecting PBel neurons attenuated 2MT-evoked hypothermia and tail temperature increment. Moreover, TeLC-mediated blockage of neurotransmission in the NTS-projecting PSTh neurons blunted 2MT-evoked hypothermia and abrogated tail temperature increase. Thus, our results identify a novel PBel-PSTh-NTS neural pathway that mediates 2MT-evoked innate fear associated hypothermia and tail vasodilation. Interestingly, Matsuo and colleagues found that chemogenetic activation of the NTS-PB pathway could also induce hypothermia[35], suggesting the potential existence of a PB-PSTh-NTS-PB feedforward loop for 2MT-evoked hypothermia. Furthermore, they also reported that trigeminal, vagal, or olfactory ablation could partially suppress 2MT-evoked hypothermia[62]. Taken together, these results suggest that multiple neural pathways may work collaboratively to mediate 2MT-evoked hypothermia.

PSTh is a novel nucleus for emotion-related thermoregulation

The subthalamic nucleus (STN) is a well-known target for deep brain stimulation to treat motor deficiency in Parkinson's disease (PD) patients[58,59]. Interestingly, deep brain stimulation of STN can trigger either motor or non-motor effects in PD patients depending on the electrode position within STN[68-71]. Recent studies suggest that STN contains a subpopulation of neurons for

processing emotion-related information[72-75]. Moreover, single-neuron recording has identified these STN neurons that respond to emotional stimuli, such as presentation of affective pictures[76]. Here, we observed that exposure to innate fear odor 2MT dramatically induced c-fos expression in the posterior part of STN, called PSTh (Fig. 1i and 1j), although it is unclear whether these 2MT-activated PSTh neurons are the same STN neurons that respond to emotional stimuli. Because PSTh neurons receive direct axonal projections from 2MT-activated PBel neurons (Fig. 6b and 6m), it is plausible that these PSTh neurons are involved in the processing of 2MT-evoked innate fear signals. Furthermore, we found that 2MT-activated PSTh neurons directly project to NTS (Fig. 2b), a critical node for autonomic regulation and thermoregulation, further supporting the idea that PSTh contains a neural population responsible for emotion-related thermoregulation. Thus, our study identifies PSTh as a novel thermoregulatory hub that connects PBel to NTS to mediate innate fear-associated hypothermia. Future studies are warranted to investigate whether PSTh is also involved in other emotion-related and patho/physiological thermoregulatory processes.

How does PSTh-NTS regulate tail vasodilation?

The two major autonomic responses to reduce body temperature are the suppression of brown adipose tissue (BAT)-dependent thermogenesis and facilitation of heat dissipation from glabrous skin, such as from the tail in rodents[3]. Matsuo and colleagues recently discovered that 2MT-evoked hypothermia was independent of suppression of BAT thermogenesis[35]. In this study, we found that 2MT exposure induced a sharp (up to 6 ºC) increase in the tail temperature

accompanying the rapid reduction in the skin and core body temperature in wild-type mice (Fig. 1b-1h). Because it is well-known that vasodilation induces heat dissipation from the skin[1,3], we expect that heat dissipation from the mouse tail contributes critically to 2MT-evoked hypothermia.

The vasomotor is controlled by the spinal sympathetic preganglionic neurons through sympathetic ganglion neurons. The rostral raphe pallidus nucleus (rRpa) is the core nucleus regulating the activity of sympathetic preganglionic neurons for controlling cutaneous vasculature, and inhibition of rRpa results in vasodilation[77]. If 2MT-evoked tail vasodilation were mediated by inhibition of rRpa, we would expect that 2MT-induced c-fos expression might be reduced in wild-type mice relative to *Trpa1*$^{-/-}$ mice. However, we observed a similar number of c-fos expressing neurons in the rRPa of wild-type and *Trpa1*$^{-/-}$ mice (Supplementary Fig. 1j), suggesting that rRpa may not play a critical role in 2MT-evoked tail vasodilation.

Alternatively, the RVLM is one of the presynaptic nuclei of spinal sympathetic preganglionic neurons for regulating cutaneous vasomotor control[3,43]. Activation of RVLM elicits vasoconstriction and increases blood pressure[43,78], whereas suppression of RVLM activity induces vasodilation[43]. The CVLM, one of the presynaptic nuclei of RVLM, plays a pivotal role in vasomotor control[43,44]. Excitation of the CVLM inhibitory neurons induces vasodilation through suppression of the neural activity in RVLM. Interestingly, CVLM receives direct synaptic input from NTS[43,44], which is strongly activated by 2MT exposure (Fig. 1i and 1j). Accordingly, we observed significant more c-fos expressing neurons in CVLM of wild-type mice than *Trpa1*$^{-/-}$ mice (Supplementary Fig. 1l), and less c-fos expressing neurons in RVML in wild-type mice than *Trpa1*$^{-/-}$ mice (Supplementary Fig. 1k).

These observations are consistent with the idea that 2MT-activated NTS neurons may induce tail vasodilation by regulating the CVLM-RVLM vasomotor control pathway.

Biological significance of innate fear-associated hypothermia

Different types of stress or fear stimuli trigger a combination of defensive behaviors and physiological responses, including thermoregulation, to promote animal survival in perceived dangerous conditions. In general, stress/fear-induced hyperthermia is a far more common phenomenon than stress/fear-induced hypothermia. For instance, short duration of physical stress, such as social defeat, tail pinch and restrain stress, induce hyperthermia[9]. Both learned fear and mild innate fear stimuli, such as ferret or fox odorants, induce hyperthermia in rodents [25,26,27]. On the other hand, potent stress or fear stimuli that threaten the survival of animals, such as long-lasting immobile stress and hypoxia, induces hypothermia[9,28-30]. Moreover, potent innate fear odor 2MT can trigger acute hypothermia accompanying robust defensive behaviors, such as freezing[33,34,35]. Thus, it is plausible that extreme stress or fear stimuli may induce hypothermia to promote animal survival, although the biological significance of stress/fear-evoked hypothermia is unclear. It has recently been shown that 2MT exposure induces potent bioprotective effects against hypoxia and ischemia/reperfusion injuries of the skin and brain by inducing hypothermia, anaerobic metabolism, and anti-inflammatory effects[35]. Thus, innate fear/stress-associated hypothermia may have evolved as a physiological defensive strategy against potent threats for animal survival. Finally, therapeutic hypothermia, i.e. lowering a person's body temperature to 32 to 34 ºC, is widely used to reduce the

risk of brain swelling, blood clots, and seizures after cardiac arrest and during heart surgery[79,80]. Thus, it may be highly beneficial to develop small molecules that can evoke innate fear-associated hypothermia and other bio-protective effects for therapeutic purposes in humans.

ACKNOWLEDGEMENTS

We thank Dr. Yoan Cherasse for sharing reagents, Drs. Takeshi Sakurai and Michael Lazarus for comments on our manuscript. This work was supported by the Beijing Municipal Science & Technology Commission (Z181100001318004 to Q.L) and the National Key Research and Development Program of China, and by the JSPS KAKENHI grants (15K14874 and 17H06048 to Q.L.; 18K06515, 18H04684 and 19H05006 to K.S; 17K08133 and 20K06738 to L.C.; 18H04806 to K.K; 18H02546 and 20H04849 to R.K.), Canon Foundation (to K.K.), the Takeda Science Foundation (to R.K. and K.K.), and the World Premier International Research Center Initiative (WPI) from MEXT, Japan.

Materials and Methods

Animals

Animal protocols used in this study were approved by the International Institute for Integrative Sleep Medicine at University of Tsukuba, Japan and by the National Institute of Biological Sciences, Beijing, China. Mice were housed in groups of 4–5 and maintained on a 12-h light-dark schedule (lights on at 9:00) with *ad libitum* access to food and water. C57BL/6J mice were obtained from CLEA, Japan. *Trpa1*$^{-/-}$ (stock 006401), Fos^{TVA} (stock 027831), and *vGlut2-IRES-Cre* (stock 016963) mice were purchased from the Jackson Laboratory (Bar Harbor, ME), United States. We used ≥ 8 weeks old male mice for all experiments.

Body temperature recording

The skin and core body temperatures were recorded by infrared digital thermographic camera (H2640, NIPPON AVIONICS) or by telemetry transmitter (TA11TA-F10, DSI), respectively. To measure the skin temperature, the back hair was shaved under anesthesia with isoflurane one day before experiments. Skin temperature was continuously recorded at 1 frame/sec, and the highest temperature in one frame was used as the skin temperature of the animal for analysis according to the user manual (InfRec Analyzer; NIPPON AVIONICS). We manually analyzed the tail temperature every 60 frames. The tail temperature is measured at the point 1 cm away from the base of the tail. To measure the core body temperature, the telemetry transmitter was implanted in the peritoneal cavity under anesthesia with isoflurane more than seven days before experiments. The core body

temperature was continuously measured upon 2MT (Tokyo Chemical Industry) exposure or optogenetic stimulation. Test mice were singly housed one day before 2MT experiment. Individual mouse was habituated for 30 min in the temperature recording cage (17.5 × 10.5 × 15 cm) placed in a fume hood. After 10 min with no odor exposure, a filter paper soaked with 20 μl 2MT was placed at the center of the cage for 15 min. All temperature recording experiments were performed under ambient temperature at 23.5 ℃.

2MT or cinnamaldehyde exposure

The mice were singly housed one day before 2MT (Tokyo Chemical Industry) or cinnamaldehyde (Nacalai Tesque) exposure experiment. Individual mouse was habituated in a temperature recording cage (17.5 x 10.5 x 15 cm) for 30 min. After 10 min with no odor exposure, 20 μl of 2MT ($2.1x10^{-4}$ mole) or cinnamaldehyde was dropped on the filter paper (~4.0 cm^2) and placed at the center of the cage for 15 min. For c-fos immunostaining, a 2MT (20 μl) soaked filter paper was placed in the mouse's home cage for 120 min before collecting the brain samples.

Viruses

The following viruses were used for experiments: AAV2/9-hSyn-DIO-hM4Di-mCherry (Addgene, 44362), AAV2/9-EF1a-DIO-ChR2-mCherry[81], AAV2/10-EF1a-DIO-mCherry (Addgene, 50462), AAV2/retro-hSyn-ChR2-EYFP (Addgene, 26973), AAV2/Retro-hSyn-EGFP (Addgene, 50465), AAV2/9-hSyn-FLEX-TeLC-P2A-GFP[82], AAV2/9-hSyn-FLEX-EGFP (Addgene, 50457), AAV2/retro-

hSyn-Cre (Addgene, 122518), CANE-LV-Cre[61]. Both AAV and lentivirus were produced as previously described[61,81].

Stereotaxic injections and implantation of optical fiber

Mice were anesthetized with 1.5-2% isoflurane and placed in a stereotaxic frame (David kopf Instruments), and small craniotomies were made over the target brain regions. Stereotaxic coordinates of virus/CTB injection were follows: PSTh, AP −2.00 mm, ML ± 1.20 mm DV −5.10 mm; PBel, AP −4.80 mm, ML ± 1.85 mm DV −4.00 mm; NTS, AP −7.80 mm, ML ± 0.30 mm DV −4.50 mm. To reach final injection site of PBel and NTS, a small craniotomy was made at the following coordinates: PBel, AP −4.10 mm, ML ± 1.85 mm DV −4.00 mm; NTS, AP −7.00 mm, ML ± 0.30 mm DV −5.70 mm. In addition, the virus/CTB injection pipette was back toward bregma at a 10 degree angle relative to vertical to inject into PBel and NTS. The virus or CTB was injected at a slow flow rate (100 nl/min) by using a pulled thin glass pipette to avoid potential damage in the injection site. The pipette was withdrawn at least 10 min after viral injection. For implantation of optical fibers (Custom-made: Diameter, 200 μm; NA, 0.22), implants were lowered above the target sites and secured to the skull with Resin Cement (3M RelyX Unicem 2). The coordinate of optical fiber implantation was follows: PSTh, AP −2.00 mm ML ± 1.20 mm DV −4.50 mm; PBel, AP −4.10 mm ML ± 1.85 mm DV −3.80 mm; RNTS, AP −6.20 mm ML ± 0.3 mm DV −4.40 mm; CNTS, AP −7.00 mm ML ± 0.4 mm DV −4.50 mm. The optical fiber was back toward bregma at a 10 degree angle relative to vertical to implant into PBel and NTS.

Capturing 2MT-activated neurons in PBel using the CANE method

To stably express ChR2 in 2MT activated PBel, singly housed Fos^{TVA} mouse was exposed 2MT (20 μl with filter paper) for 15 min. Around 45 min later, the Fos^{TVA} mouse was lightly anesthetized with isoflurane and fixed in stereotaxic flame. By following previously described virus injection method, the mixture of CANE-Lv-Cre and AAV2/9-EF1a-DIO-ChR2-mCherry or AAV2/10-EF1a-DIO-mCherry were injected into PBel.

Optogenetic and chemogenetic experiments

To activate ChR2 labeled neurons, blue light was delivered by a laser (473nm; Shanghai Laser & Optics Century). Before optogenetic stimulation, the mice were lightly anesthetized with isoflurane and a ferrule patch cord (Doric Lenses) was connected to ferrule optic fiber. The laser pulses were controlled through Doric Neuroscience Studio. The mice were photostimulated at 20 mW, 20 Hz, and 25 ms pulse duration for 15 minutes stimulation pattern on neurons and for 30 minutes stimulation pattern on axon terminals. For chemogenetic experiment, hM4Di or mCherry expressing mice were injected i.p. with C21 (1 mg/kg; HB6124, Hello Bio) 30 min before 2MT exposure.

Immunohistochemistry, image acquisition and quantification

Mice were deeply anesthetized with isoflurane and transcardially perfused with ice-cold 10% sucrose in Milli-Q water, followed by ice-cold and 4% paraformaldehyde (PFA) in 0.1M phosphate

buffer saline, pH 7.4 (PBS). Dissected brains were post-fixed for overnight in 4% PFA and transferred to 30% sucrose in PBS at 4°C. Then, brains were frozen in Tissue-Tek O.C.T (Sakura) and stored at -80 °C. Coronal brain slices (80 μm) were made using a cryostat (Leica Biosystems). After washing with PBS for three times, brain slices were treated with permeabilization solution (1% Triton in PBS) at room temperature for 3 hours, and followed by incubation with the Blocking buffer (10% Blocking One (Nacalai Tesque) with 0.3% Triton X-100 in PBS) at room temperature for 1 hour. Brain slices were incubated with the primary (1^{st}) antibody in Blocking buffer at 4 °C overnight. After washing with PBS three times, brain slices were incubated with secondary (2^{nd}) antibody in blocking buffer at 4 °C overnight. The slices were stained with NeuroTrace fluorescent Nissl stain (Invitrogen, N-21279) or 4', 6-diamidino-2-phenylinodole (DAPI) (Dojindo, D523), washed, mounted and coverslipped. Immunostained brain slices were imaged using a Zeiss LSM800 confocal microscope with 10x or 20x objective lens. Antibodies information: 1^{st} antibodies: Rabbit polyclonal anti-c-fos (Sigma-Aldrich, ABE457), Goat polyclonal anti-mCherry (SCIGEN, AB0040-200), Rat monoclonal anti-GFP (Nacalai tesque, 04404-84); All 2^{nd} antibodies were obtained from Jackson ImmunoResearch: Donkey anti-rabbit Alexa Fluor 488 (711-545-152), Donkey anti-rabbit Cy3 (711-165-152), Donkey anti-rat Alexa Fluor 488(712-545-153), Donkey anti-goat Cy3 (705-165-147).

Cell counting and quantification

Images were analyzed by Image J or Adobe Photoshop counting tool. For the c-fos mapping experiments, cell density of c-fos positive neurons in each region was calculated. In each brain

region, we randomly selected 3-5 brain slices and manually outlined the target nucleus. The area of the target nucleus was calculated automatically by Image J. Then, we counted the number of c-fos positive neurons inside the outline and calculated the cell density of c-fos positive neurons by dividing the area in each section. The final cell density of c-fos positive neurons in each region was the average cell density among sections containing the target region in each mouse. Quantification of the two color fluorescence in situ hybridization results (the cell number and the ratio of *c-fos*+, *vGlut2*+ or *c-fos*+, *vGAT*+ double positive neurons) and the number of CTB-based retrograde labeling results (the cell number and the ratio of c-fos+, CTB+ double positive neurons) were performed as same as c-fos mapping experiments which described above. The final percentage of each population was the average percentage among sections containing the target region in each mouse. To quantify the ratio of TeLC-expressing neurons in PSTh, the number of TeLC+ neurons and the total number of DAPI signals in PSTh were similarly counted as described above. The infection rate of each mouse indicates the percentage of TeLC+ neurons in PSTh.

Two color in situ hybridization

The cDNA fragments of mouse *c-fos*, *vGlut2*, and *vGAT* genes were amplified by PCR with antisense primers containing T7 promoter sequence. In vitro transcription was performed with PCR-amplified templates using T7 RNA polymerase (Roche) to synthesize antisense RNA probes. Two-color in situ hybridization was performed based on a basic method (Ishii et al., 2017). Briefly, mice were exposed 2MT for 30 min, deeply anesthetized with isoflurane, and transcardially perfused with

ice-cold 10% sucrose in MilliQ water followed by ice-cold 4% PFA. The collected brain samples were post-fixed with 4% PFA at 4 °C overnight, followed by displacement with 30% sucrose in PBS containing 0.1% Diethylpyrocarbonate (DEPC) at 4 °C overnight. Coronal brain sections (40 µm) were made using a cryostat (Leica Biosystems). Brain sections were treated with proteinase K (Roche) followed by acetylation, and then incubated with hybridization buffer containing antisense RNA probes at 60 °C for 16 hours. After stringent washing, brain sections were incubated with horseradish peroxidase (HRP) conjugated anti-FITC antibody (PerkinElmer; 1:1000) or HRP-conjugated anti-Dig antibody (Roche; 1:1000) at 4 °C overnight. To sequentially use HRP-conjugated antibody, 2% sodium azide solution was treated for inactivation of HRP. TSA system (TSA-FITC and TSA-Biotin; PerkinElmer) and Streptavidin Alexa Fluor 568 conjugate (ThermoFisher) were used to visualize the mRNA signals.

Statistics

For statistical analyses of the experimental data, two-sided Student's t-test, two way ANOVA analysis and linear regression analysis were used. The n used for these analyses represents the number of mice. Detailed information on statistical analyses is provided in the figure legends.

REFERENCES

1 Morrison, S. F. & Nakamura, K. Central Mechanisms for Thermoregulation. *Annual Review of Physiology* **81** (2019).

2 Madden, C. J. & Morrison, S. F. Central nervous system circuits that control body temperature. *Neuroscience Letters* **696**, 225-232, doi:10.1016/j.neulet.2018.11.027 (2019).

3 Tan, C. L. & Knight, Z. A. Regulation of Body Temperature by the Nervous System. *Neuron*, doi:10.1016/j.neuron.2018.02.022 (2018).

4 Morrison, S. F. Central neural control of thermoregulation and brown adipose tissue. *Autonomic Neuroscience: Basic and Clinical*, doi:10.1016/j.autneu.2016.02.010 (2016).

5 Tansey, E. A. & Johnson, C. D. Recent advances in thermoregulation. *Advances in Physiology Education* **39**, 139-148, doi:10.1152/advan.00126.2014 (2015).

6 Seebacher, F. & Franklin, C. E. Physiological mechanisms of thermoregulation in reptiles: A review. *Journal of Comparative Physiology B: Biochemical, Systemic, and Environmental Physiology* **175**, 533-541, doi:10.1007/s00360-005-0007-1 (2005).

7 Huey, R. B. Temoerature, Physiology, and the ecology of Reptile. *Deep-Sea Research Part I: Oceanographic Research Papers* **92**, 127-140, doi:10.1016/j.dsr.2014.07.003 (2008).

8 Kataoka, N., Shima, Y., Nakajima, K. & Nakamura, K. A central master driver of psychosocial stress responses in the rat. *Science* **367**, 1105-1112, doi:10.1126/science.aaw7182 (2020).

9 Oka, T. Stress-induced hyperthermia and hypothermia. *Handbook of Clinical Neurology* **157**, 599-621, doi:10.1016/B978-0-444-64074-1.00035-5 (2018).

10 Oka, T. Psychogenic fever: how psychological stress affects body temperature in the clinical population. *Temperature* **2**, 368-378, doi:10.1080/23328940.2015.1056907 (2015).

11 Nakamura, K. Central circuitries for body temperature regulation and fever. *American Journal of Physiology - Regulatory Integrative and Comparative Physiology*, doi:10.1152/ajpregu.00109.2011 (2011).

12 Evans, S. S., Repasky, E. A. & Fisher, D. T. Fever and the thermal regulation of immunity: The immune system feels the heat. *Nature Reviews Immunology* **15**, 335-349, doi:10.1038/nri3843 (2015).

13 Sunagawa, G. A. & Takahashi, M. Hypometabolism during Daily Torpor in Mice is Dominated by Reduction in the Sensitivity of the Thermoregulatory System. *Scientific Reports* **6**, 1-14, doi:10.1038/srep37011 (2016).

14 Heldmaier, G., Ortmann, S. & Elvert, R. Natural hypometabolism during hibernation and daily torpor in mammals. *Respiratory Physiology and Neurobiology*, doi:10.1016/j.resp.2004.03.014 (2004).

15 Geiser, F. Metabolic Rate and Body Temperature Reduction During Hibernation and Daily Torpor. *Annual Review of Physiology*, doi:10.1146/annurev.physiol.66.032102.115105 (2004).

16 Webb, G. P., Jagot, S. A. & Jakobson, M. E. Fasting-induced torpor in Mus musculus and its implications in the use of murine models for human obesity studies. *Comparative Biochemistry and Physiology -- Part A: Physiology* **72**, 211-219, doi:10.1016/0300-9629(82)90035-4 (1982).

17 Kozlowska, K., Walker, P., McLean, L. & Carrive, P. Fear and the Defense Cascade: Clinical Implications and Management. *Harvard Review of Psychiatry* **23**, 263-287, doi:10.1097/HRP.0000000000000065 (2015).

18 Roelofs, K. Freeze for action: Neurobiological mechanisms in animal and human freezing. *Philosophical Transactions of the Royal Society B: Biological Sciences* **372**, doi:10.1098/rstb.2016.0206 (2017).

19 Silva, B. A., Gross, C. T. & Gr?Ff, J. The neural circuits of innate fear: detection, integration, action, and memorization. *Learning & Memory* **23**, 544-555 (2016).

20 Gross, C. T. & Canteras, N. S. The many paths to fear. *Nature Reviews Neuroscience* **13**, 651-685, doi:10.1038/nrn3301 (2012).

21 Sladek, C. D., Michelini, L. C., Stachenfeld, N. S., Stern, J. E. & Urban, J. H. Endocrine-autonomic linkages. *Comprehensive Physiology*, doi:10.1002/cphy.c140028 (2015).

22 Ulrich-Lai, Y. M. & Herman, J. P. Neural regulation of endocrine and autonomic stress responses. *Nature Reviews Neuroscience*, doi:10.1038/nrn2647 (2009).

23 Keay, K. A. & Bandler, R. Parallel circuits mediating distinct emotional coping reactions to different types of stress. *Neuroscience and Biobehavioral Reviews* **25**, 669-678, doi:10.1016/S0149-7634(01)00049-5 (2001).

24 Schipper, P., Hiemstra, M., Bosch, K., Nieuwenhuis, D. & Adinolfi, A. The association between serotonin transporter availability and the neural correlates of fear bradycardia. *Proceedings of the National Academy of ences* **116**, 201904843, doi:10.1073/pnas.1904843116 (2019).

25 Vianna, D. M. & Carrive, P. Changes in cutaneous and body temperature during and after conditioned fear to context in the rat. *The European journal of neuroscience* **21**, 2505-2512, doi:10.1111/j.1460-9568.2005.04073.x (2005).

26 Horii, Y., Nagai, K. & Nakashima, T. Order of exposure to pleasant and unpleasant odors affects autonomic nervous system response. *Behavioural Brain Research* **243**, 109-117, doi:10.1016/j.bbr.2012.12.042 (2013).

27 Campeau, S., Nyhuis, T. J., Sasse, S. K., Day, H. E. W. & Masini, C. V. Acute and chronic effects of ferret odor exposure in Sprague-Dawley rats. *Neuroscience and Biobehavioral Reviews* **32**, 1277-1286, doi:10.1016/j.neubiorev.2008.05.014 (2008).

28 Wood, S. Interactions Between Hypoxia And Hypothermia. *Annual Review of Physiology* **53**, 71-85, doi:10.1146/annurev.physiol.53.1.71 (1991).

29 Amar, A. & Sanyal, A. K. Immobilization stress in rats: Effect on rectal temperature and possible role of brain monoamines in hypothermia. *Psychopharmacology*, doi:10.1007/BF00429208 (1981).

30 GRANT, R. Emotional hypothermia in rabbits. *The American journal of physiology*, doi:10.1152/ajplegacy.1950.160.2.285 (1950).

31 Ginsburg, G. S., Riddle, M. A. & Davies, M. Somatic symptoms in children and adolescents with anxiety disorders. *Journal of the American Academy of Child and Adolescent Psychiatry* **45**, 1179-1187, doi:10.1097/01.chi.0000231974.43966.6e (2006).

32 Shioiri, T., Someya, T., Murashita, J. & Takahashi, S. The symptom structure of panic disorder: A trial using factor and cluster analysis. *Acta Psychiatrica Scandinavica* **93**, 80-86, doi:10.1111/j.1600-0447.1996.tb09806.x (1996).

33 Wang, Y. *et al.* Large-scale forward genetics screening identifies Trpa1 as a chemosensor for predator odor-evoked innate fear behaviors. *Nature Communications*, doi:10.1038/s41467-018-04324-3 (2018).

34 Isosaka, T. *et al.* Htr2a-Expressing Cells in the Central Amygdala Control the Hierarchy between Innate and Learned Fear. *Cell*, doi:10.1016/j.cell.2015.10.047 (2015).

35 Matsuo, T. *et al.* Thiazoline-related TRPA1 agonist odorants orchestrate survival fate in mice. *bioRxiv* (2020).

36 Mei, J. *et al.* Body temperature measurement in mice during acute illness: Implantable temperature transponder versus surface infrared thermometry. *Scientific Reports* **8**, 1-10, doi:10.1038/s41598-018-22020-6 (2018).

37 Meyer, C. W., Ootsuka, Y. & Romanovsky, A. A. Body Temperature Measurements for Metabolic Phenotyping in Mice. *Frontiers in Physiology*, doi:10.3389/fphys.2017.00520 (2017).

38 Gordon, C. J. Thermal biology of the laboratory rat. *Physiology and Behavior* **47**, 963-991, doi:10.1016/0031-9384(90)90025-Y (1990).

39 Tovote, P., Fadok, J. P. & Lüthi, A. Neuronal circuits for fear and anxiety. *Nature Reviews Neuroence*.

40 Tupone, D., Madden, C. J. & Morrison, S. F. Central activation of the A1 adenosine receptor (A1AR) induces a hypothermic, torpor-like state in the rat. *Journal of Neuroscience* **33**, 14512-14525, doi:10.1523/JNEUROSCI.1980-13.2013 (2013).

41 Cao, W. H., Madden, C. J. & Morrison, S. F. Inhibition of brown adipose tissue thermogenesis by neurons in the ventrolateral medulla and in the nucleus tractus solitarius. *American Journal of Physiology - Regulatory Integrative and Comparative Physiology* **299**, 277-290, doi:10.1152/ajpregu.00039.2010 (2010).

42 Madden, C. J. & Morrison, S. F. Hypoxic activation of arterial chemoreceptors inhibits sympathetic outflow to brown adipose tissue in rats. *Journal of Physiology* **566**, 559-573, doi:10.1113/jphysiol.2005.086322 (2005).

43 Schreihofer, A. M. & Guyenet, P. G. The baroreflex and beyond: Control of sympathetic vasomotor tone by gabaergic neurons in the ventrolateral medulla. *Clinical and Experimental Pharmacology and Physiology* **29**, 514-521, doi:10.1046/j.1440-1681.2002.03665.x (2002).

44 Sved, A. F., Ito, S. & Madden, C. J. Baroreflex dependent and independent roles of the caudal ventrolateral medulla in cardiovascular regulation. *Brain Research Bulletin* **51**, 129-133, doi:10.1016/S0361-9230(99)00234-8 (2000).

45 Pautrat, A. *et al.* Revealing a novel nociceptive network that links the subthalamic nucleus to pain processing. *eLife*, doi:10.7554/eLife.36607 (2018).

46 Takahashi, T. M., Sunagawa, G. A., Soya, S., Abe, M. & Sakurai, T. A discrete neuronal circuit induces a hibernation-like state in rodents. *Nature* (2020).

47 Hrvatin, S., Sun, S., Wilcox, O. F., Yao, H. & Greenberg, M. E. Neurons that regulate mouse torpor. *Nature* **583**, 1-7 (2020).

48 Morrison, S. F. & Nakamura, K. Central neural pathways for thermoregulation. *Front Biosci (Landmark Ed)* **16** (2011).

49 Tan, C. L. *et al.* Warm-Sensitive Neurons that Control Body Temperature. *Cell* **167**, 47-59.e15, doi:10.1016/j.cell.2016.08.028 (2016).

50 Chiang, M. C. *et al.* Divergent Neural Pathways Emanating from the Lateral Parabrachial Nucleus Mediate Distinct Components of the Pain Response. *Neuron*, 1-13, doi:10.1016/j.neuron.2020.03.014 (2020).

51 Palmiter, R. D. The Parabrachial Nucleus: CGRP Neurons Function as a General Alarm. *Trends in Neurosciences*, doi:10.1016/j.tins.2018.03.007 (2018).

52 Chen, J. Y., Campos, C. A., Jarvie, B. C. & Palmiter, R. D. Parabrachial CGRP Neurons Establish and Sustain Aversive Taste Memories. *Neuron* **100**, 891-899.e895, doi:10.1016/j.neuron.2018.09.032 (2018).

53 Rodriguez, E. *et al.* A craniofacial-specific monosynaptic circuit enables heightened affective pain. *Nature Neuroscience* **20**, 1734-1743, doi:10.1038/s41593-017-0012-1 (2017).

54 Shen, W. L., Xu, X. & Yang, H. Parabrachial neuron types categorically encode thermoregulation variables during heat defense. *Science Advances* **6**, 36 (2020).

55 Geerling, J. C. *et al.* Genetic identity of thermosensory relay neurons in the lateral parabrachial nucleus. *American Journal of Physiology - Regulatory Integrative and Comparative Physiology*, doi:10.1152/ajpregu.00094.2015 (2016).

56 Chan Lek *et al.* Warm-Sensitive Neurons that Control Body Temperature. *Cell* (2016).

57 Nambu, A. *et al.* Excitatory conical inputs to pallidal neurons via the subthalamic nucleus in the monkey. *Journal of Neurophysiology* **84**, 289-300, doi:10.1152/jn.2000.84.1.289 (2000).

58 Schuepbach, W. M. M. *et al.* Neurostimulation for Parkinson's disease with early motor complications. *New England Journal of Medicine* **368**, 610-622, doi:10.1056/NEJMoa1205158 (2013).

59 P Limousin 1 , P. K., P Pollak, A Benazzouz, C Ardouin, D Hoffmann, A L Benabid. Electrical Stimulation of the Subthalamic Nucleus in Advanced Parkinson's Disease. *New England Journal of Medicine* **339**, 1105-1111 (1998).

60 Tschida, K. *et al.* Article A Specialized Neural Circuit Gates Social Vocalizations in the Mouse Article A Specialized Neural Circuit Gates Social Vocalizations in the Mouse. *Neuron* **103**, 459-471.e455, doi:10.1016/j.neuron.2019.05.025 (2019).

61 Sakurai, K. *et al.* Capturing and Manipulating Activated Neuronal Ensembles with CANE Delineates a Hypothalamic Social-Fear Circuit. *Neuron*, S0896627316307164, doi:10.1016/j.neuron.2016.10.015 (2016).

62 Tomohiko Matsuo, T. I., Yuichiro Hayashi, Lijun Tang,, Akihiro Doi, M. H., Chia-Ying Lee, Liqin Cao, Natsumaro Kutsuna,, Sachihiro Matsunaga, T. M., Ikuko Yao, Mitsuyoshi Setou, Dai, Kanagawa, K. H., Masahito Ikawa, Qinghua Liu, Reiko & Kobayakawa, K. K. TRPA1 commands intrinsic bioprotective effects of innate fear odors. *Nature Communications* (In submission) (2020).

63 Kalia, M. & Sullivan, J. M. Brainstem projections of sensory and motor components of the vagus nerve in the rat. *Journal of Comparative Neurology* **211**, 248-264, doi:10.1002/cne.902110304 (1982).

64 Henssen, D. J. H. A. *et al.* New insights in trigeminal anatomy: A double orofacial tract for nociceptive input. *Frontiers in Neuroanatomy* **10**, 1-14, doi:10.3389/fnana.2016.00053 (2016).

65 Rodriguez, E. *et al.* A craniofacial-specific monosynaptic circuit enables heightened affective pain. *Nature Neuroence*.

66 Slugg, R. M. & Light, A. R. Spinal cord and trigeminal projections to the pontine parabrachial region in the rat as demonstrated with Phaseolus vulgaris leucoagglutinin. *Journal of Comparative Neurology* **339**, 49-61, doi:10.1002/cne.903390106 (1994).

67 Cechetto, D. F., Standaert, D. G. & Saper, C. B. Spinal and trigeminal dorsal horn projections to the parabrachial nucleus in the rat. *Journal of Comparative Neurology* **240**, 153-160, doi:10.1002/cne.902400205 (1985).

68 Růžička, F. *et al.* Chronic stress-like syndrome as a consequence of medial site subthalamic stimulation in Parkinson's disease. *Psychoneuroendocrinology* **52**, 302-310, doi:10.1016/j.psyneuen.2014.12.001 (2015).

69 Welter, M. L. *et al.* Optimal target localization for subthalamic stimulation in patients with Parkinson disease. *Neurology* **82**, 1352-1361, doi:10.1212/WNL.0000000000000315 (2014).

70 Růžička, F. *et al.* Weight gain is associated with medial contact site of subthalamic stimulation in parkinson's disease. *PLoS ONE* **7**, 1-7, doi:10.1371/journal.pone.0038020 (2012).

71 Herzog, J. *et al.* Most effective stimulation site in subthalamic deep brain stimulation for Parkinson's disease. *Movement Disorders* **19**, 1050-1054, doi:10.1002/mds.20056 (2004).

72 Wagenbreth, C., Kuehne, M., Heinze, H. J. & Zaehle, T. Deep Brain Stimulation of the Subthalamic Nucleus Influences Facial Emotion Recognition in Patients With Parkinson’s Disease: A Review. *Frontiers in Psychology* **10**, 1-14, doi:10.3389/fpsyg.2019.02638 (2019).

73 Castrioto, A., Lhommée, E., Moro, E. & Krack, P. Mood and behavioural effects of subthalamic stimulation in Parkinson's disease. *The Lancet Neurology* **13**, 287-305, doi:10.1016/S1474-4422(13)70294-1 (2014).

74 Mallet, L. *et al.* Stimulation of subterritories of the subthalamic nucleus reveals its role in the integration of the emotional and motor aspects of behavior. *Proceedings of the National Academy of Sciences of the United States of America* **104**, 10661-10666, doi:10.1073/pnas.0610849104 (2007).

75 Temel, Y., Blokland, A., Steinbusch, H. W. M. & Visser-Vandewalle, V. The functional role of the subthalamic nucleus in cognitive and limbic circuits. *Progress in Neurobiology* **76**, 393-413, doi:10.1016/j.pneurobio.2005.09.005 (2005).

76 Sieger, T. *et al.* Distinct populations of neurons respond to emotional valence and arousal in the human subthalamic nucleus. *Proceedings of the National Academy of Sciences of the United States of America* **112**, 3116-3121, doi:10.1073/pnas.1410709112 (2015).

77 Blessing, W., Mcallen, R. & Mckinley, M. Control of the Cutaneous Circulation by the Central Nervous System. *Comprehensive Physiology* **6**, 1161 (2016).

78 MORRISON, S. F. Differential Regulation of Sympathetic Outflows to Vasoconstrictor and Thermoregulatory Effectors. *Annals of the New York Academy of Sciences* **940**, 286-298, doi:10.1111/j.1749-6632.2001.tb03684.x (2006).

79 Sherer, M. & Novack, T. A. Neuropsychological Assessment After Traumatic Brain Injury in Adults. *Clinical Neuropsychology and Cost Outcome Research* **289**, 39-60, doi:10.4324/9781315787039-4 (2020).

80 Holzer, M. *et al.* Mild therapeutic hypothermia to improve the neurologic outcome after cardiac arrest. *New England Journal of Medicine* **346**, 549-556, doi:10.1056/NEJMoa012689 (2002).

81 Oishi, Y. *et al.* Slow-wave sleep is controlled by a subset of nucleus accumbens core neurons in mice. *Nature Communications* **8**, 1-12, doi:10.1038/s41467-017-00781-4 (2017).

82 Zhang, Y. *et al.* Identifying local and descending inputs for primary sensory neurons. *Journal of Clinical Investigation*, doi:10.1172/JCI81156 (2015).

FIGURES

Figure 1. Innate fear odor 2MT induces hypothermia and tail temperature increase via Trpa1.

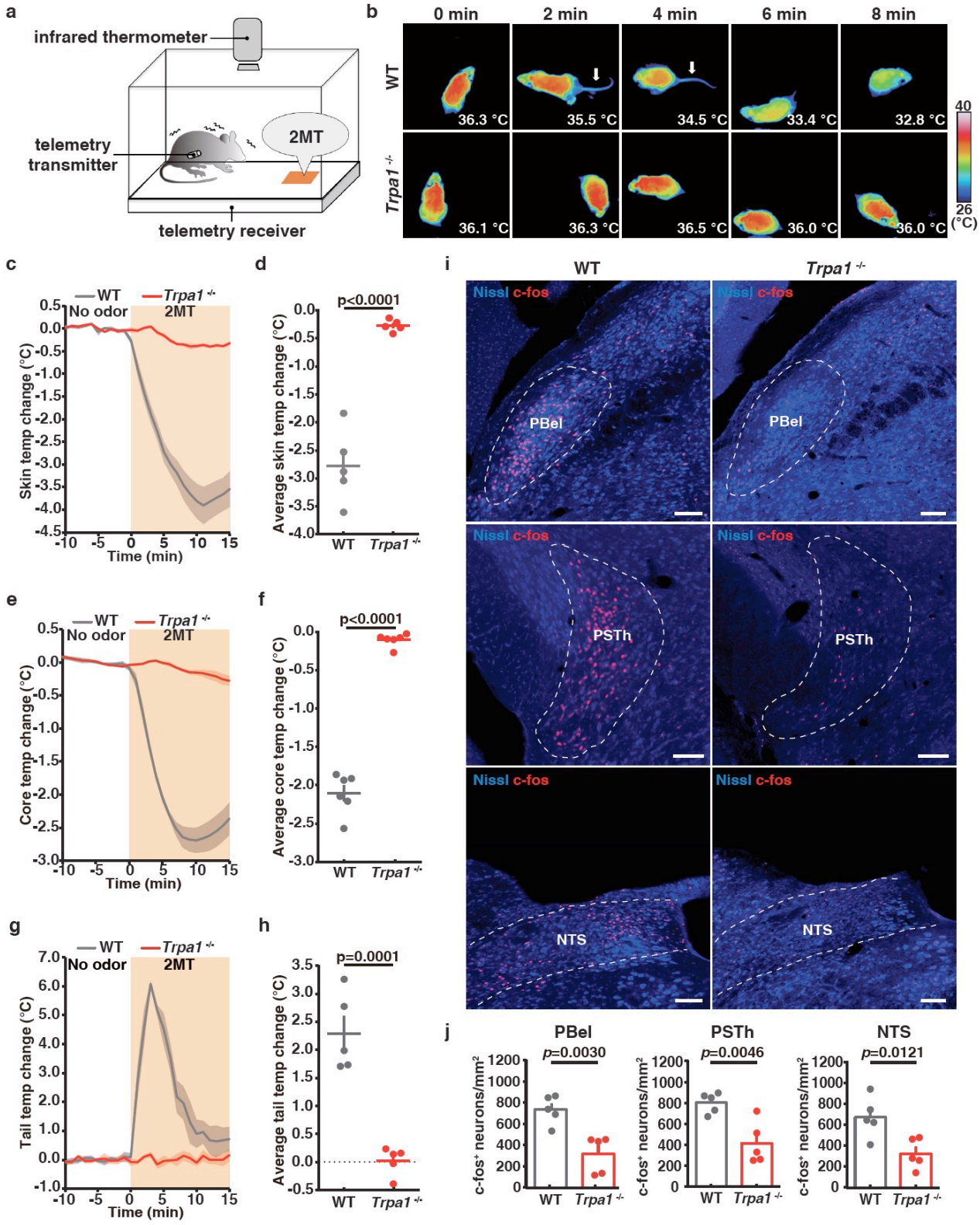

Figure 1 Innate fear odor 2MT induces hypothermia and tail temperature increase *via* Trpa1.

a Schematic of 2MT-induced hypothermia assay in mice. **b** Time-lapsed thermal images showing tail and skin temperature changes in wild-type (upper) and *Trpa1*$^{-/-}$ (bottom) mice during 2MT treatment. **c, e, g** Tail (**c**), skin (**e**) and core (**g**) body temperature curves of wild-type and *Trpa1*$^{-/-}$ mice (n=5 or 6) before and during 2MT treatment. **d, f, h** Average tail (**d**), skin (**f**) and core (**h**) body temperature changes of wild-type and *Trpa1*$^{-/-}$ mice during 2MT treatment. **i,** Representative images showing 2MT-induced c-Fos expression in PBel, PSTh and NTS of wild-type and *Trpa1*$^{-/-}$ mice. **j,** Quantitative analysis of 2MT-evoked c-Fos expression in PBel, PSTh and NTS in wild-type and *Trpa1*$^{-/-}$ mice (n=5). (**c-h, j**) Data are mean ± SEM; two-side Student's t test. Scale bars, 100 μm.

Figure 2. Inhibition of vGlut2 + PSTh neurons attenuates 2MT-evoked hypothermia and tail temperature increase.

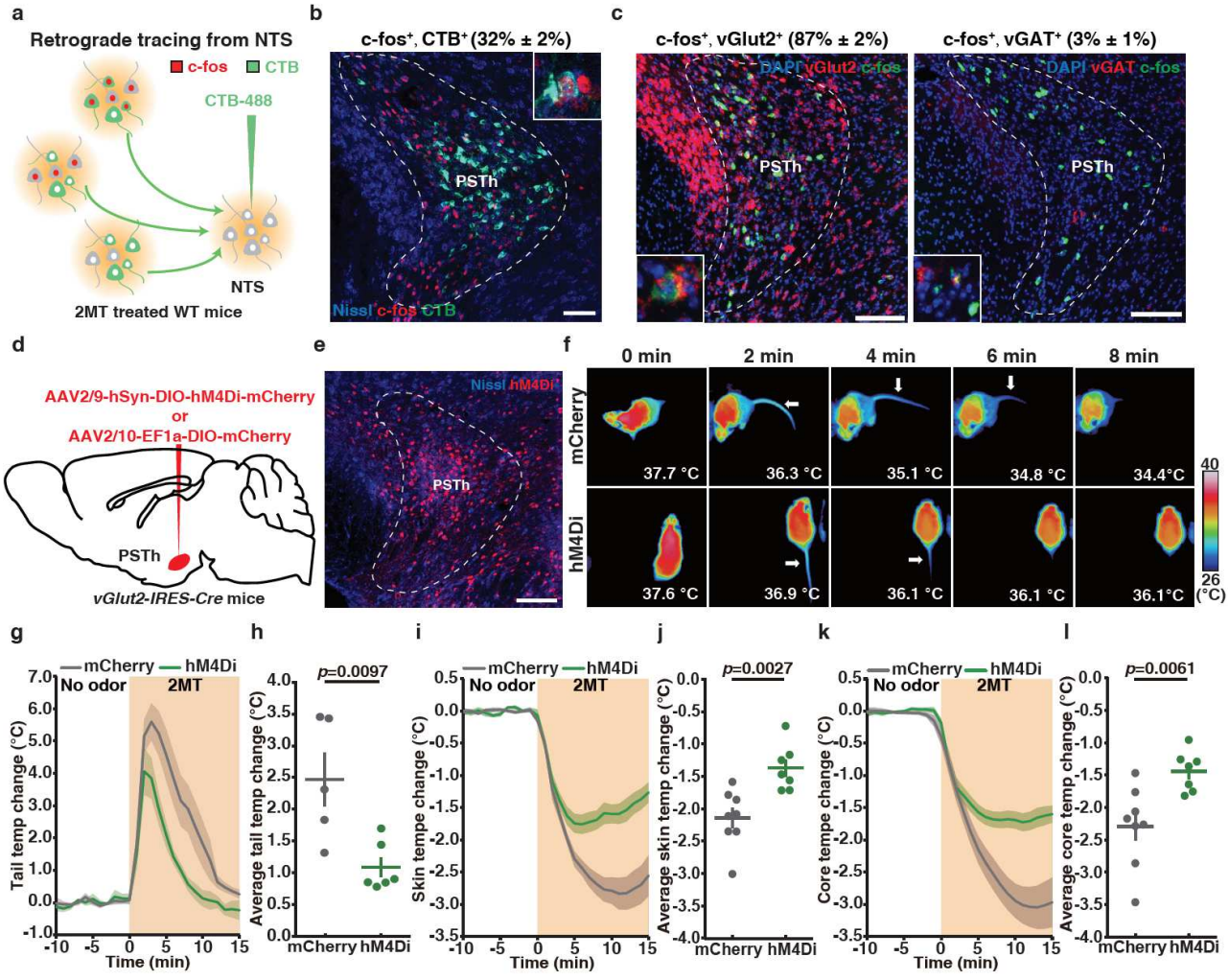

Figure 2. Inhibition of vGlut2$^+$ PSTh neurons attenuates 2MT-evoked hypothermia and tail temperature increase.

a Schematic of retrograde tracing from NTS neurons by CTB injection. **b,** Representative image showing double immunostaining of CTB and c-fos. The percentage of double positive neurons (CTB$^+$, c-fos$^+$/CTB$^+$%) in PSTh is in parenthesis. **c** Representative images and quantitative analysis showing the percentage of *c-fos*$^+$, *vGlut2*$^+$ or *c-fos*$^+$, *vGAT*$^+$ double positive neurons among *c-fos*$^+$ neurons in PSTh by two color in situ hybridization. **d** Schematic of chemogenetic inhibition experiment of vGlut2$^+$ PSTh neurons in *vGlut2-IRES-Cre* mice. **e** Representative image of hMD4i-labeled vGlut2$^+$ PSTh neurons. **f** Time-lapsed thermal images of mCherry-expressing mice and hM4Di-expressing mice during 2MT treatment following administration of C21. **g, i, k** Tail (**g**), skin (**i**) and core (**k**) temperature curves of mice with (hM4Di, n=7) or without (mCherry, n=8) inactivation of vGlut2$^+$ PSTh neurons before and during 2MT treatment. **h, j, l** Average tail (**h**), skin (**j**) and core (**l**) temperature changes of mice with (hM4Di) or without (mCherry) inactivation of vGlut2$^+$ PSTh neurons during 2MT treatment. A few mice were not included in the analysis of tail temperature (e) because their tails were frequently obscured in the thermal images. **(g-l)** Data are mean ± SEM; two-side Student's t test. Scale bars, 100 μm.

Figure 3. TeLC-mediated inactivation of NTS-projecting PSTh neurons diminishes 2MT-evoked hypothermia and abrogates tail temperature increase.

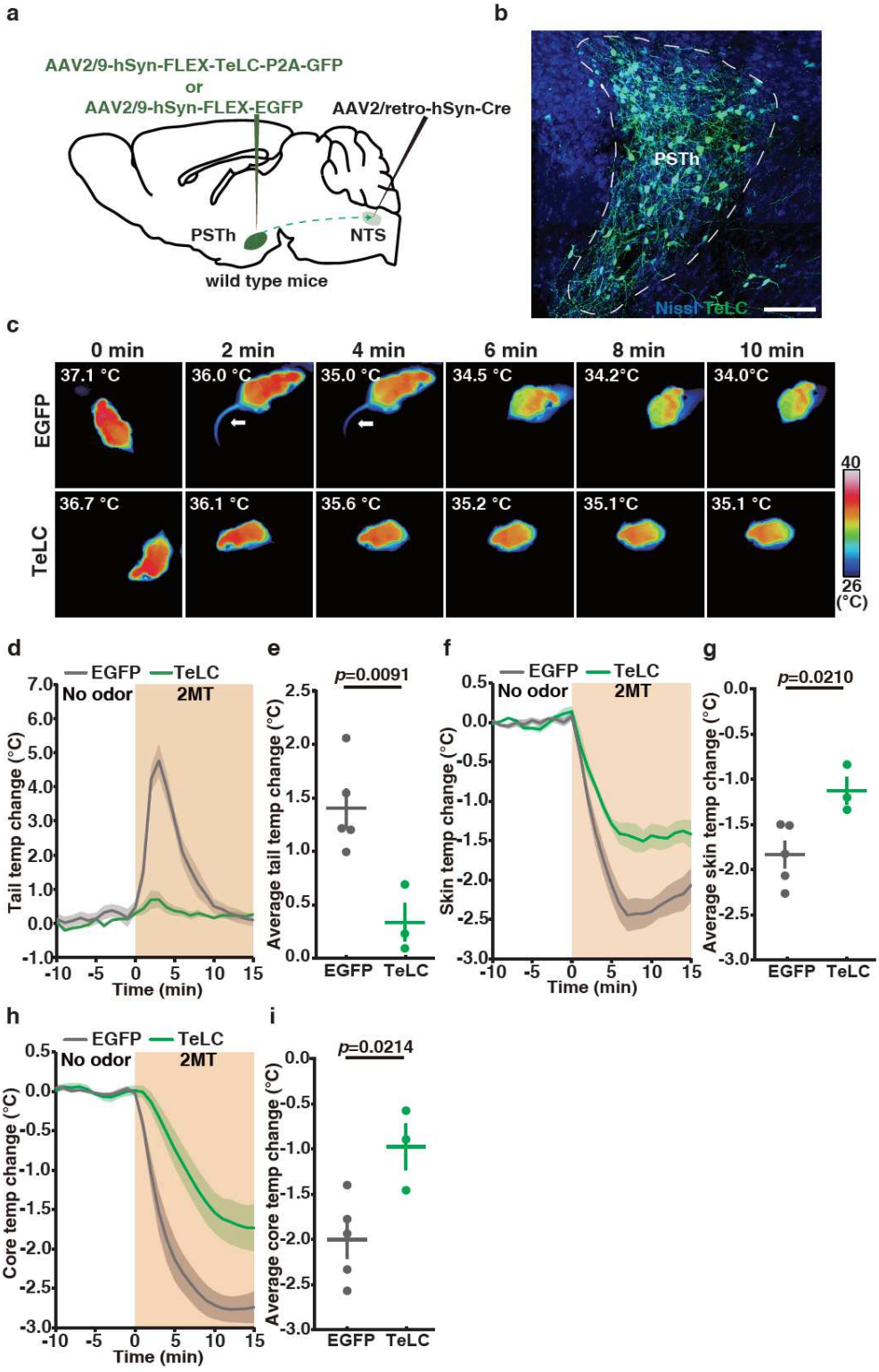

Figure 3 TeLC-mediated inactivation of NTS-projecting PSTh neurons diminishes 2MT-evoked hypothermia and abrogates tail temperature increase.

a Schematic of TeLC-mediated inactivation of PSTh neurons in wild-type mice. **b** Representative image showing TeLC-GFP-labeled NTS-projecting PSTh neurons. **c** Time-lapsed thermal images of wild-type mice without (EGFP, up) or with (TeLC, bottom) inactivation of NTS-projecting PSTh neurons during 2MT treatment. **d, f, h** Tail (**d**), skin (**f**) and core (**h**) temperature curves of EYFP-expressing (n=5) and TeLC-expressing (n=3) mice before and during 2MT treatment. **e, g, i** Average tail (**e**), skin (**g**) and core (**i**) temperature changes of EGFP-expressing and TeLC-expressing mice during 2MT treatment. Two TeLC-expressing mice were not included in the analysis because of low virus transduction rate (Supplementary Fig. 3). **(d-i)** Data are mean ± SEM; two-side Student's t test. Scale bar, 100 μm.

Figure 4. Activation of NTS-projecting PSTh neurons evokes hypothermia and tail temperature increase.

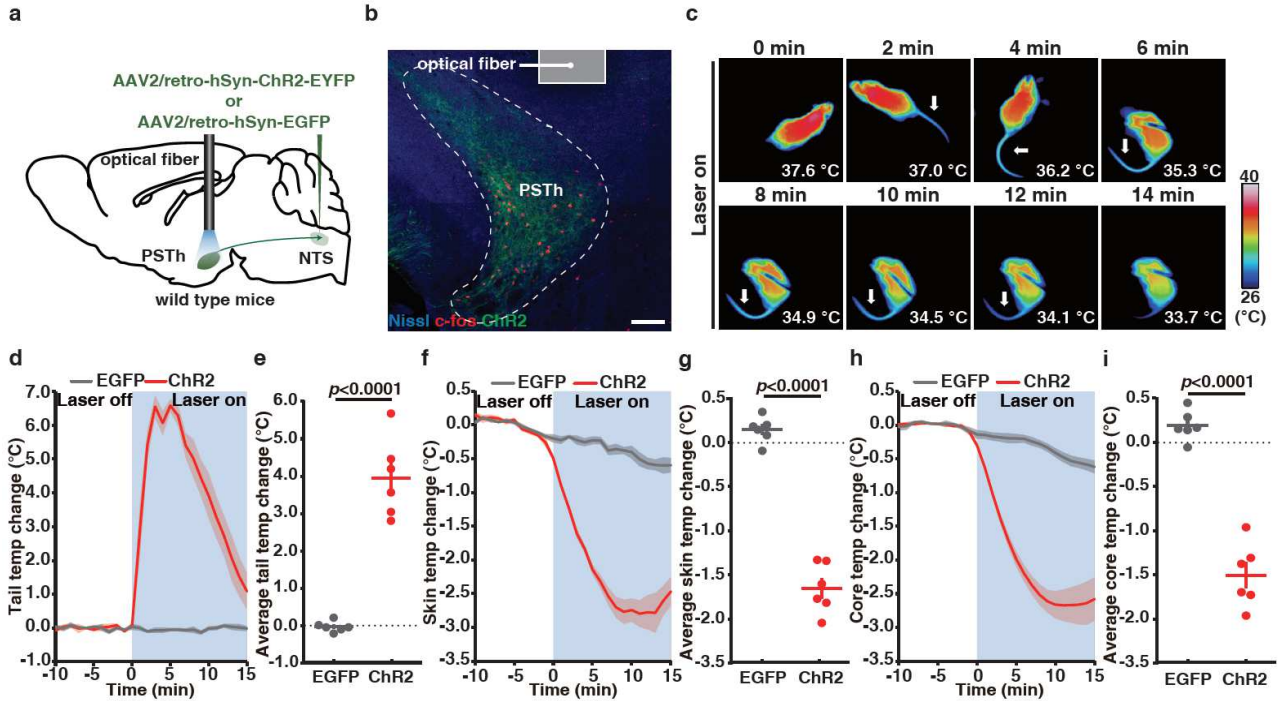

Figure 4. Activation of NTS-projecting PSTh neurons evokes hypothermia and tail temperature increase.

a Schematic of optogenetic activation of the PSTh-NTS pathway in wild-type mice. **b** Representative image showing c-fos expression in ChR2-labeled PSTh neurons after photoactivation. **c** Time-lapsed thermal images of ChR2-expressing mice during photoactivation of the NTS-projecting PSTh neurons. **d, f, h** Tail (**d**), skin (**f**) and core (**h**) temperature curves of EGFP-expressing (n=6) and ChR2-expressing mice (n=6) before and during photoactivation of the NTS-projecting PSTh neurons. **e, g, i** Average tail (**e**), skin (**g**) and core (**i**) temperature changes of EGFP-expressing and ChR2-expressing mice during photoactivation of NTS-projecting PSTh neurons. (**d-i**) Data are mean ± SEM; two-side Student's t test. Scale bar, 100 μm.

Figure 5. RNTS but not CNTS is the main target for hypothermia evoking PSTh neurons.

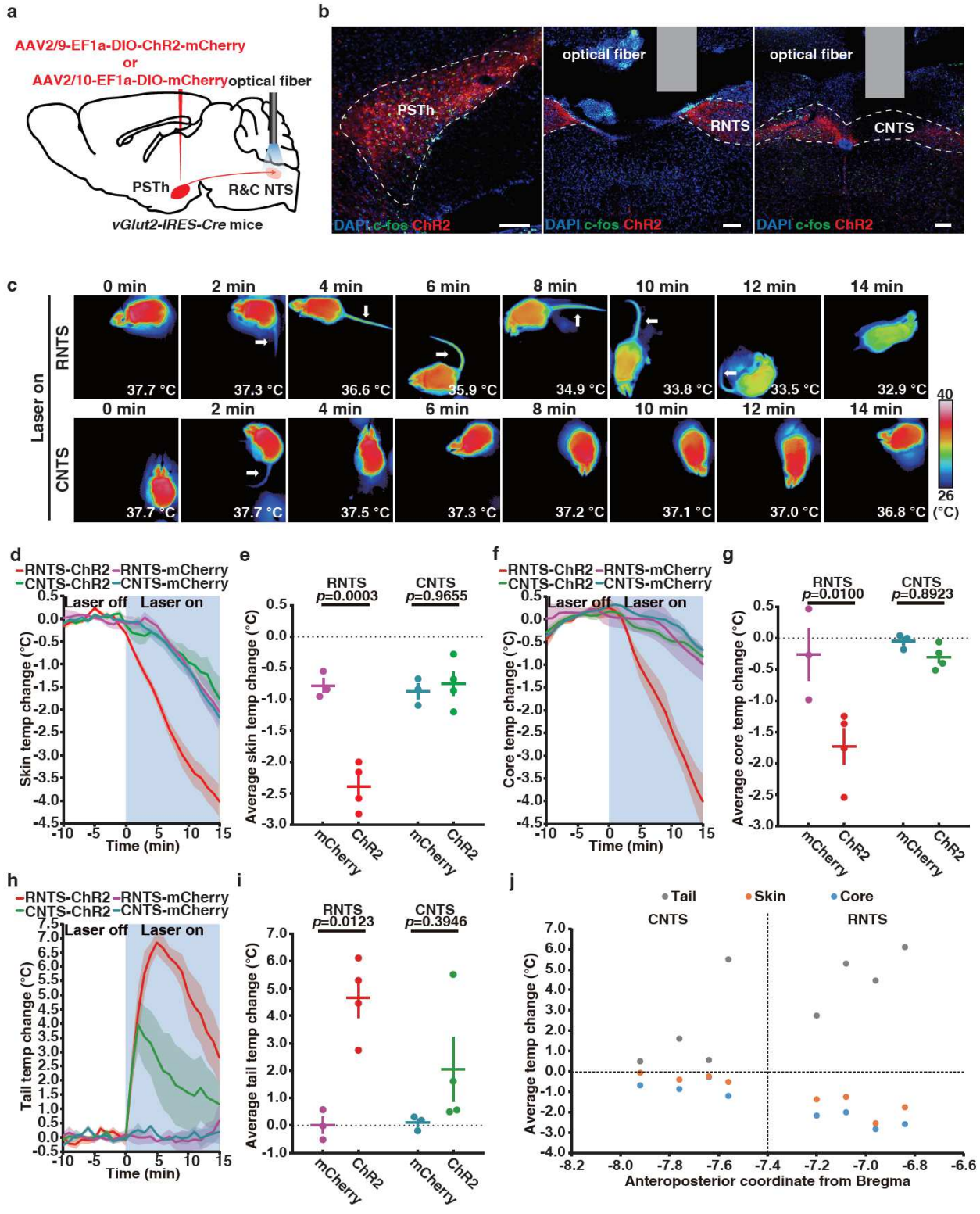

Figure 5 RNTS, but not CNTS, is the main target for hypothermia evoking PSTh neurons.

a Schematic of optogenetic activation of the PSTh-NTS pathway in wild-type mice. **b** Representative images showing c-fos expression in ChR2-labeled PSTh neurons (left) and their axon terminals in RNTS (middle) and CNTS (right) in *vGlut2-IRES-Cre* mice after photoactivation. **c** Time-lapsed thermal images of ChR2-expressing mice during photoactivation of axon terminals of RNTS- or CNTS-projecting PSTh neurons. **d, f, h** skin (**d**), core (**f**) and tail (**h**) temperature curves of mCherry-expressing (n=3) and ChR2-expressing mice (n=4) before and during photoactivation of axon terminals of RNTS- or CNTS-projecting PSTh neurons. **e, g, i** Average skin (**e**), core (**g**) and tail (**i**) temperature changes of mCherry-expressing and ChR2-expressing mice during photoactivation of axon terminals of RNTS- or CNTS-projecting PSTh neurons. **j** Correlative analysis between the photoactivation-induced average tail, skin and core temperature changes in ChR2-expressing mice and the anteroposterior coordinates of the optical fiber implant sites. (**d-i**) Data are mean ± SEM; two way ANOVA analysis followed by Tukey's multiple comparisons test. Scale bars, 100 μm.

Figure 6. Activation of 2MT activated PBel neurons and their axonal inputs to PSTh evokes hypothermia.

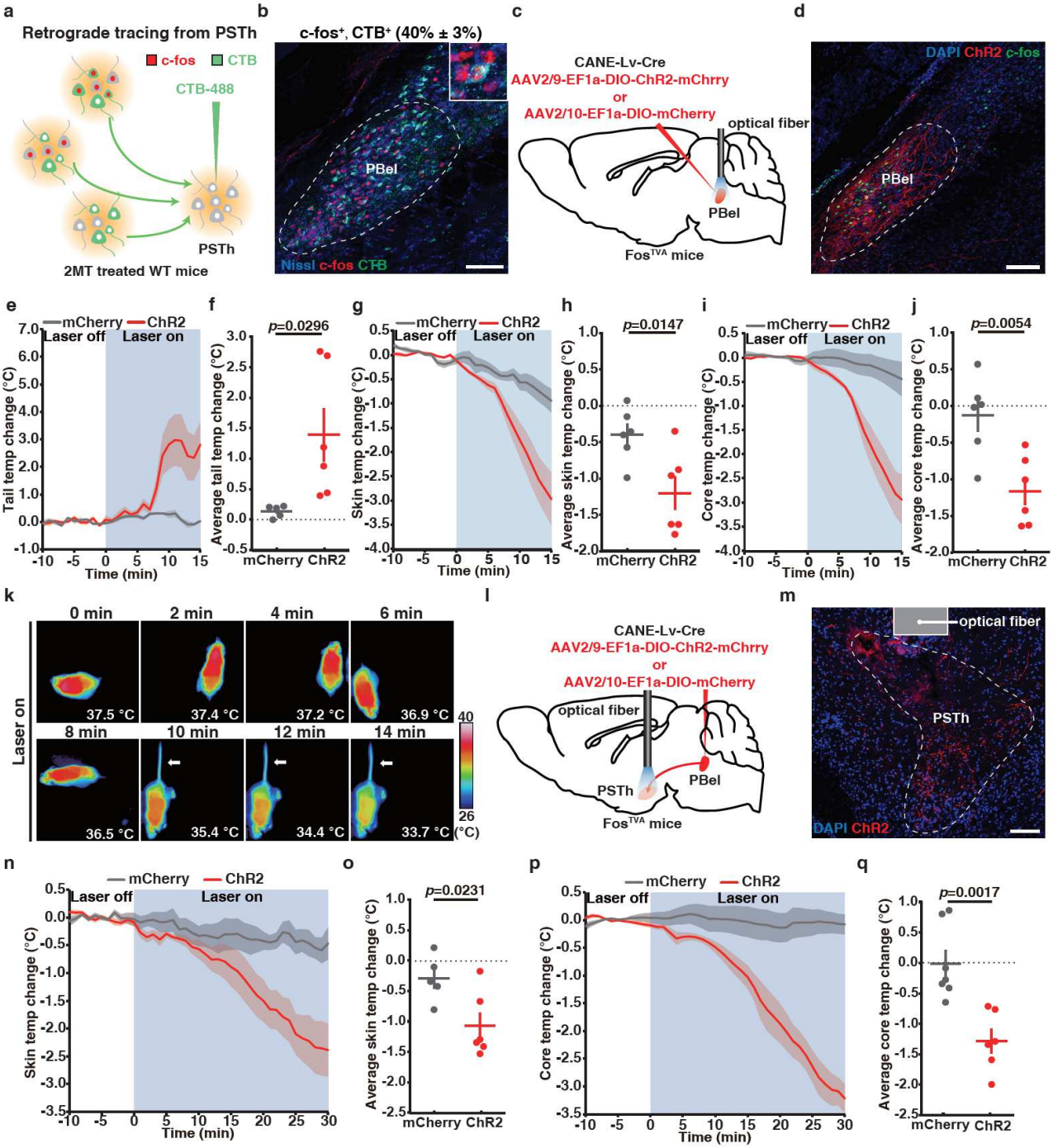

Figure 6 Activation of 2MT-activated PBel neurons and their axonal inputs to PSTh evokes hypothermia.

a Schematic of retrograde tracing from PSTh neurons by CTB. **b** Representative images showing double immunostaining of CTB and c-fos. The percentage of c-fos$^+$, CTB$^+$ neurons among CTB$^+$ neurons in PBel is shown in parenthesis. **c** Schematic of selective opto-stimulation of the cell bodies of 2MT-activated PBel neurons labeled by CANE in Fos^{TVA} mice. d. Representative images showing c-fos expression in the ChR2-labeled PBel neurons following photoactivation. **e, g, i** Tail (**e**), skin (**g**) and core (**i**) temperature curves of mCherry-expressing (n=5 or 7) and ChR2-expressing (n=6) Fos^{TVA} mice before and during blue light stimulation of 2MT-activated PBel neurons. **f, h, i** Average tail (**f**), skin (**h**) and core (**j**) temperature changes of mCherry-expressing and ChR2-expressing Fos^{TVA} mice during opto-stimulation of 2MT-activated PBel neurons. **k** Time-lapsed thermal images of ChR2-expressing Fos^{TVA} mice during photoactivation of 2MT-activated PBel neurons. **l** Schematic of selective opto-stimulation of the axon terminals of 2MT-activated PBel neurons in PSTh in Fos^{TVA} mice. **m** Representative images showing the ChR2-labeled axon terminals from 2MT-activated PBel neurons in PSTh. **n, p** Skin (n) and core (p) temperature curves of mCherry-expressing (n=5 or 7) and ChR2-expressing (n=6) Fos^{TVA} mice before and during blue light stimulation of axon terminals in PSTh. **o, q** Average skin (o) and core (q) temperature changes of mCherry-expressing and ChR2-expressing Fos^{TVA} mice during blue light stimulation of axon terminals in PSTh. **(e-j, n-q)** Data are mean ± SEM; two-side Student's t test. Scale bars, 100 μm

Figure 7. Inhibition of PSTh-projecting PBel neurons diminishes 2MT-evoked hypothermia.

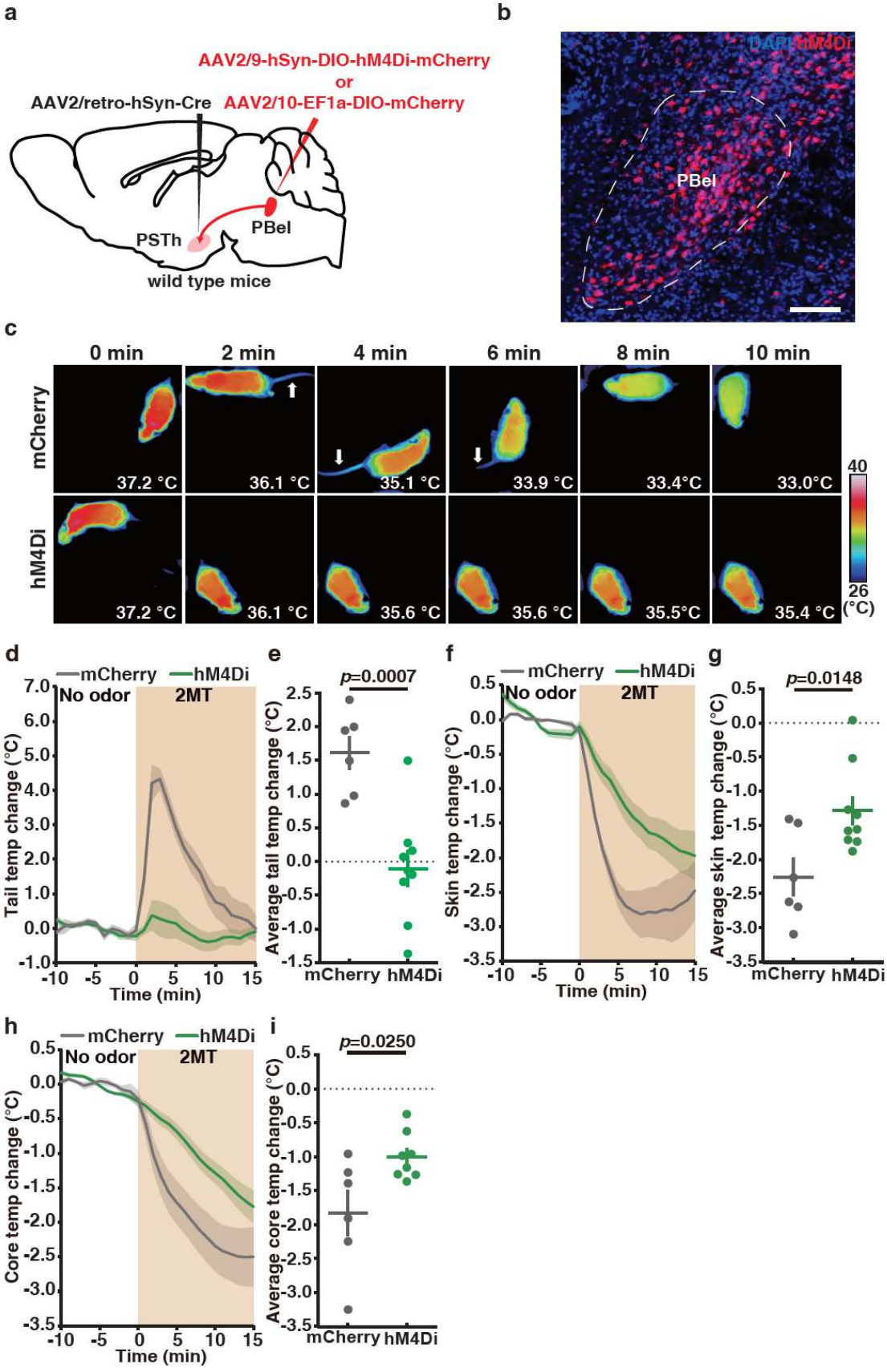

Figure 7 Inhibition of PSTh-projecting PBel neurons diminishes 2MT-evoked hypothermia and tail temperature increase.

a Schematic of chemogenetic inhibition PSTh-projecting PBel neurons. **b** Representative image of hMD4i-labeled PSTh-projecting PBel neurons. **c** Time-lapsed thermal images of mCherry-expressing mice and hM4Di-expressing mice during 2MT treatment following administration of C21. **d, f, h** Tail (**d**), skin (**f**) and core (**h**) temperature curves of mice with (hM4Di, n=8 or 9) or without (mCherry, n=6) inactivation of PSTh-projecting PBel neurons before and during 2MT treatment. **e, g, i** Average tail (**e**), skin (**g**) and core (**i**) temperature changes of mice with (hM4Di) or without (mCherry) inactivation of PSTh-projecting PBel neurons during 2MT treatment. **(d-i)** Data are mean ± SEM; two-side Student's t test. Scale bar, 100 μm.

Figure 8. Neural circuits for 2MT-evoked hypothermia.

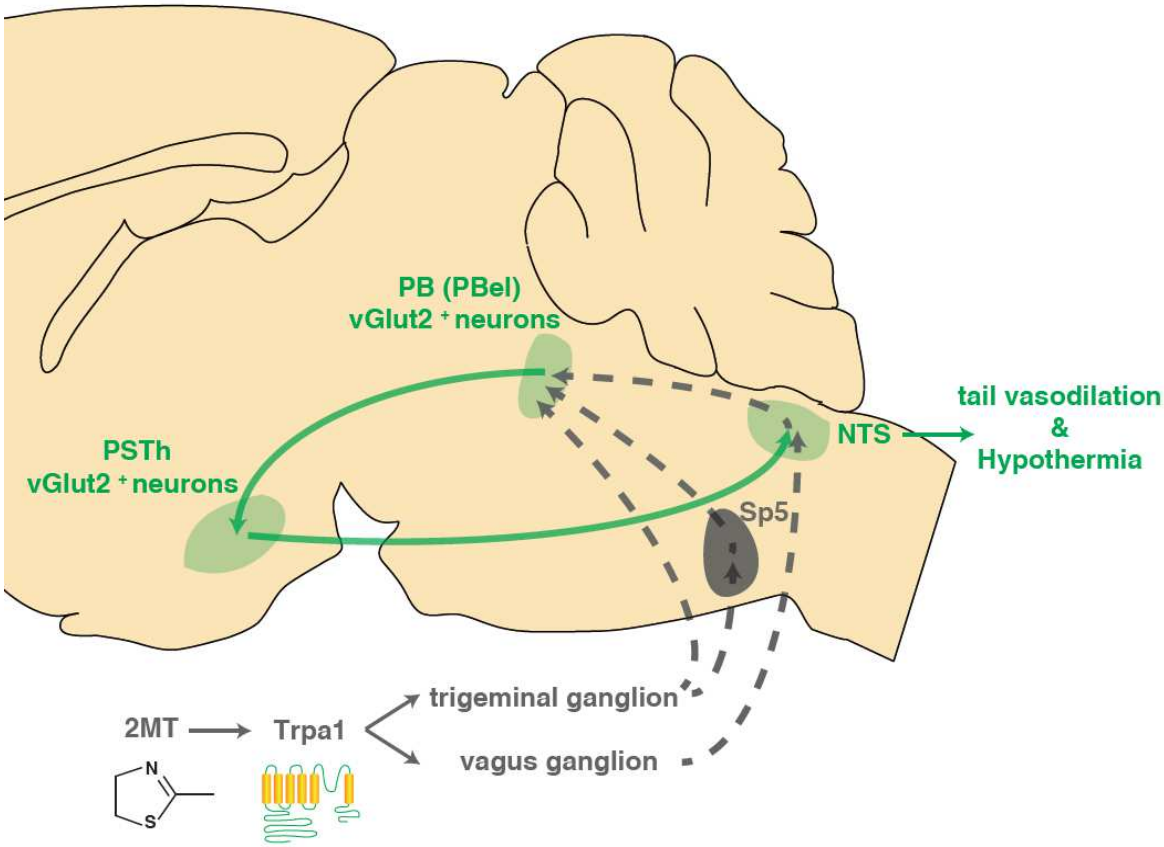

Figure 8. Neural pathways for 2MT-evoked hypothermia.

Supplementary Figure 1. *TRPA1* agonist cinnamaldehyde treatment and 2MT induced c-fos expression.

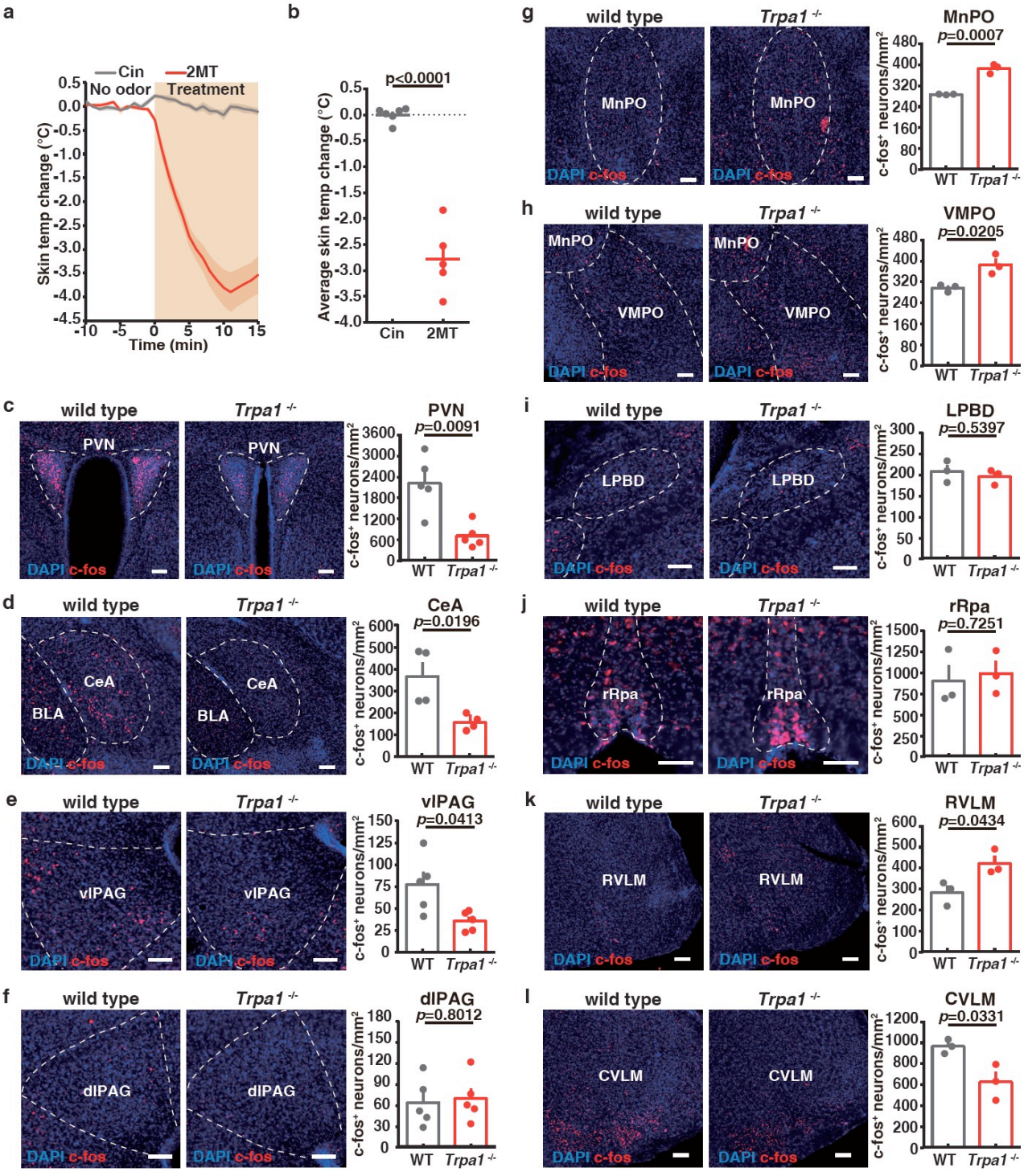

Supplementary Figure 1. TRPA1 agonist cinnamaldehyde treatment and 2MT induced c-fos expression.

a Skin temperature curves of wild-type mice before and during 2MT (n=5) or cinnamaldehyde (n=6) treatment. **b** Average skin temperature changes of wild-type during 2MT or cinnamaldehyde treatment. **c-l** Representative images and quantitative analysis of 2MT-evoked c-fos expression showing 2MT-induced c-fos expression in PVN (**c**), CeA (**d**), vlPAG (**e**), dlPAG (**f**), MnPO (**g**), VMPO (**h**), LPBD (**i**), rRpa (**j**), RVLM (**k**), CVLM (**l**) of wild-type and *Trpa1*$^{-/-}$ mice (n=3,4 or 5). Data are mean ± SEM; two-side Student's t test. Scale bars, 100 μm. Cin, cinnamaldehyde; MnPO, median preoptic nucleus; VMPO, ventromedial preoptic nucleus; PVN, paraventricular hypothalamic nucleus; CeA, central amygdala; vlPAG, ventrolateral periaqueductal gray; dlPAG, dorsolateral periaqueductal gray; LPBD, dorsal part of the lateral parabrachial nucleus; rRpa, rostral raphe pallidus nucleus; RVLM, rostral ventrolateral medulla; CVLM, caudal ventrolateral medulla.

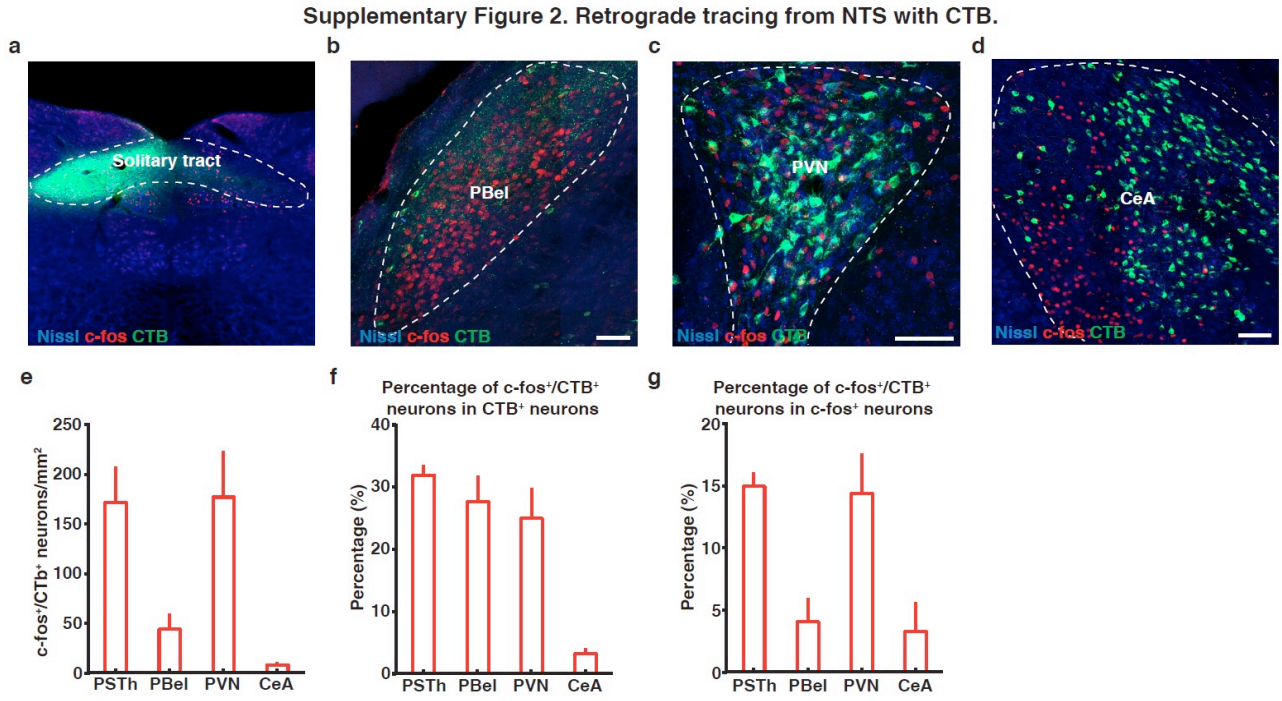

Supplementray Figure 2. Retrograde tracing from NTS with CTB.

a Representative image showing CTB injection site in NTS. **b-d** Representative images showing double immunostaining of CTB and c-fos in PBel (**b**), PVN (**c**), and CeA (**d**) (PSTh is shown in Fig. 2b). **e** Quantitative analysis of the density of c-fos$^+$, CTB$^+$ double positive neurons in various brain regions. **f** Quantitative analysis of the percentage of CTB$^+$ neurons that are also c-fos$^+$ in various brain regions. **g** Quantitative analysis of the percentage of c-fos$^+$ neurons that are also CTB$^+$ in various brain regions. **(e-g)** Data are mean ± SEM. Scale bars, 100 μm.

Supplementary Figure 3. Inhibitory effect of TeLC depends on the virus transduction rate.

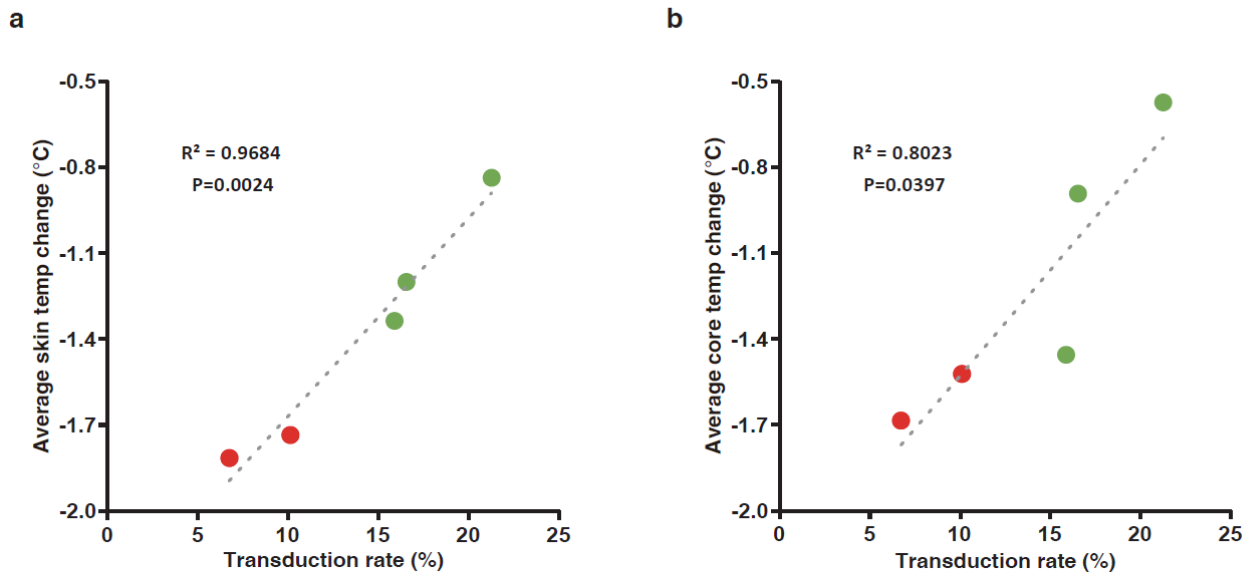

Supplementary Figure 3. Inhibitory effect of TeLC depends on the virus transduction rate.

a Quantitative analysis showing the 2MT-evoked average skin temperature reduction of TeLC-expressing mice is inversely related to the virus transduction rate. **b** Quantitative analysis showing the 2MT-evoked average core body temperature reduction of TeLC-expressing mice is inversely related to the virus transduction rate. Linear regression was used for statistical analysis. The two red dots in each graph refers to two mice with low virus transduction rate, which were not included in Figure 3.

Supplementary Figure 4. Fiber implant sites of ChR2 labled mice in NTS.

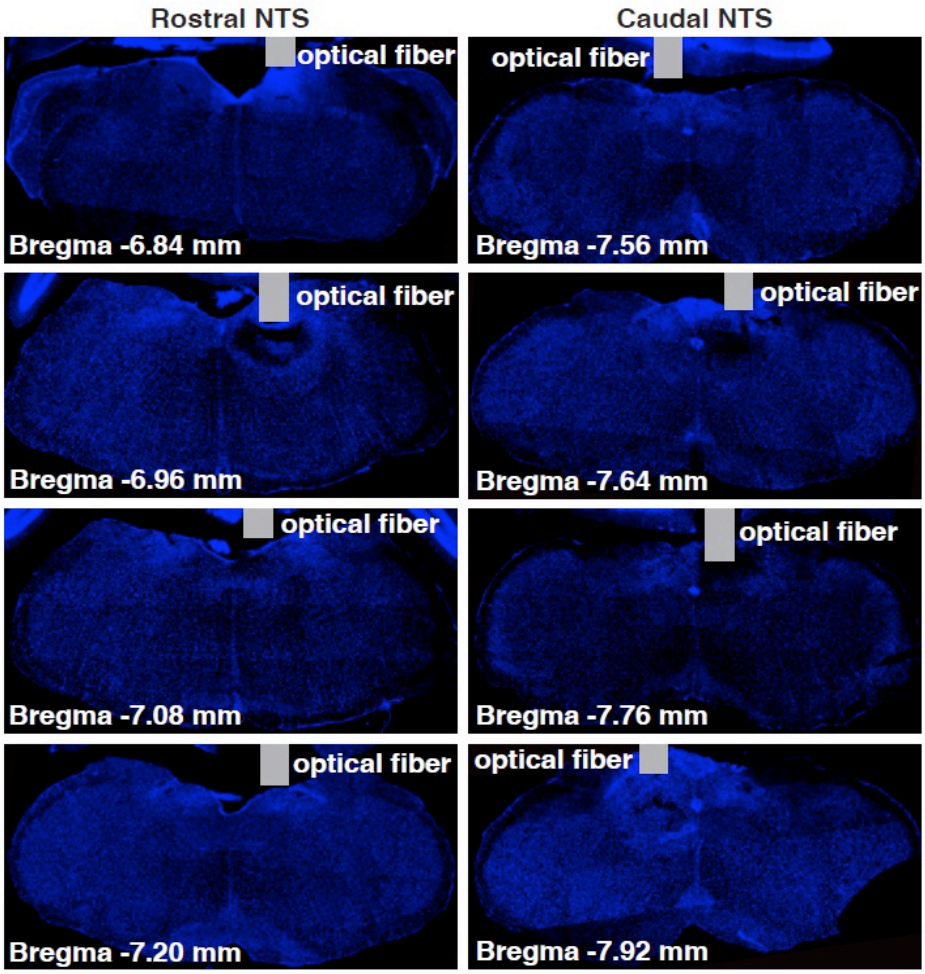

Supplementary Figure 4. Fiber implant sites of ChR2 labeled mice in NTS.

Images showing optical fiber implant site in NTS.

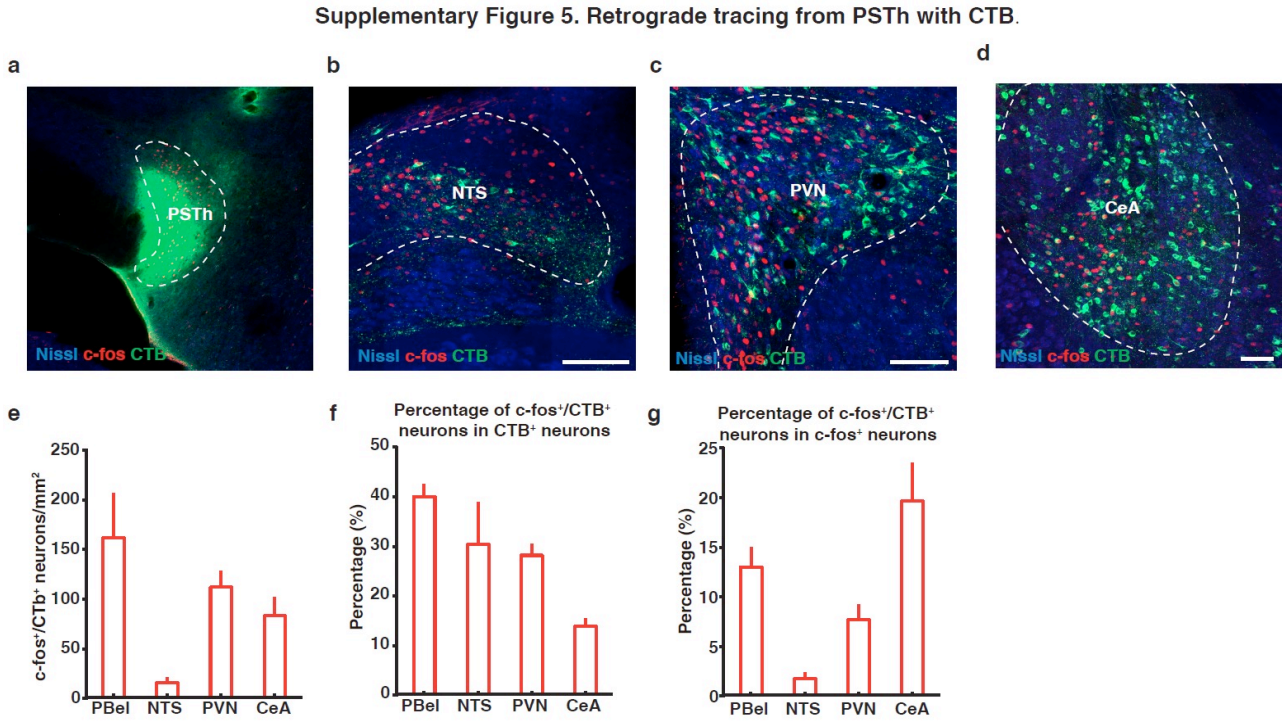

Supplementary Figure 5. Retrograde tracing from PSTh with CTB.

a Representative image showing CTB injection site in PSTh. **b-d** Representative images showing double immunostaining of CTB and c-fos in NTS (**b**), PVN (**c**), and CeA (**d**) (PBel is shown in Fig. 5b). **e** Quantitative analysis of the density of c-fos$^+$, CTB$^+$ double positive neurons in various brain regions. **f** Quantitative analysis showing the percentage of CTB$^+$ positive neurons that are also c-fos$^+$ in various brain regions. **g** Quantitative analysis of the c-fos$^+$ neurons that are also CTB$^+$ in various brain regions. **(e-g)** Data are mean ± SEM. Scale bars, 100 μm.

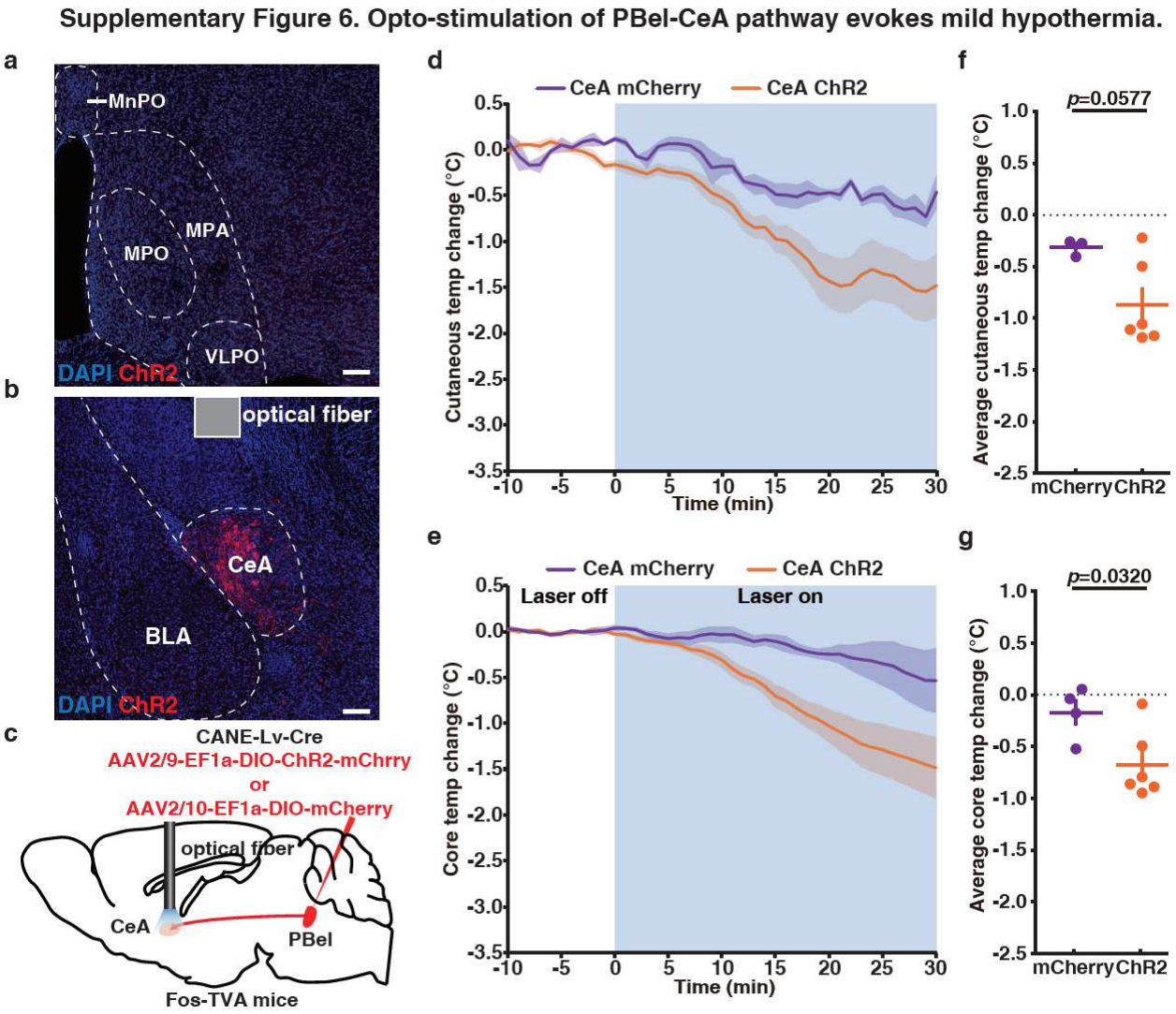

Supplementary Figure 6 Opto-stimulation of PBel-CeA pathway evokes mild hypothermia.

a, b Representative images showing that CANE-labeled PBel neurons project to CeA (b), but not POA (a) in Fos^{TVA} mice. **c** Schematic of selective opto-stimulation of the axon terminals in CeA from 2MT-activated PBel neurons labeled by CANE in Fos^{TVA} mice. **d, e** Skin (**d**) and core (**e**) temperature curves of mCherry-expressing (n=3 for skin, n=4 for core) and ChR2-expressing (n=6) Fos^{TVA} mice before and during photoactivation of the axon terminals of 2MT-activated PBel neurons in CeA. **f, g** Average skin (**f**) and core (**g**) temperature changes of mCherry-expressing and ChR2-expressing

Fos^{TVA} mice during photoactivation of the axon terminals of 2MT-activated PBel neurons in CeA. **(d-g)** Data are mean ± SEM; two-side Student's t test. Scale bars, 100 µm.

Supplementary Figure 7. Inhibition of vGlut2 + PBel neurons attenuates 2MT-evoked hypothermia.

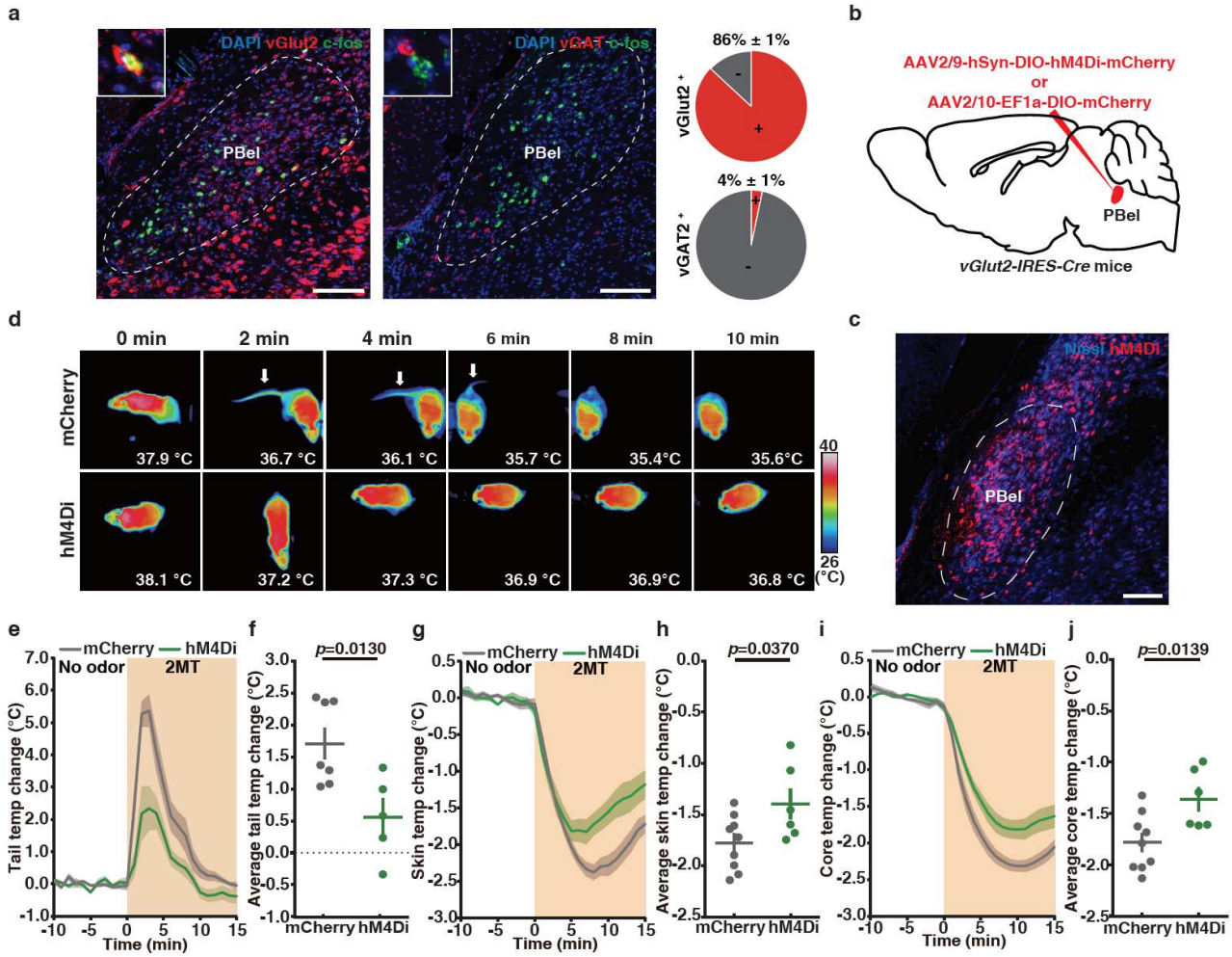

Supplementary Figure 7 Inhibition of vGlut2$^+$ PBel neurons attenuates 2MT-evoked hypothermia amd tail temperature increase.

a Representative images and quantitative analysis showing the percentage of *c-fos*$^+$*, vGlut2*$^+$ and *c-fos*$^+$*, vGAT*$^+$ double positive neurons among 2MT-activated *c-fos*$^+$ neurons in PBel by two color in situ hybridization. **b** Schematic of chemogenetic inhibition of vGlut2$^+$ PBel neurons in *vGlut2-IRES-Cre* mice. **c** Representative image showing hM4Di-labeled vGlut2$^+$ PBel neurons. **d** Time-lapsed thermal images of mCherry-expressing and hM4Di-expressing mice during 2MT treatment following administration of C21. **e, g, i** Tail (**e**), skin (**g**) and core (**i**) temperature curves of mice with (hM4Di, n=6) and without (mCherry, n=9) inactivation of vGlut2$^+$ PBel neurons before and during 2MT treatment. **f, h, j** Average tail (**f**), skin (**h**) and core (**j**) temperature changes of mice with (hM4Di) or without (mCherry) inactivation of vGlut2$^+$ PBel neurons during 2MT treatment. A few mice were not included in the analysis of tail temperature (**e, f**) because their tails were frequently obscured in the thermal images. **(e-j)** Data are mean ± SEM; two-side Student's t test. Scale bars, 100 μm.

Figures

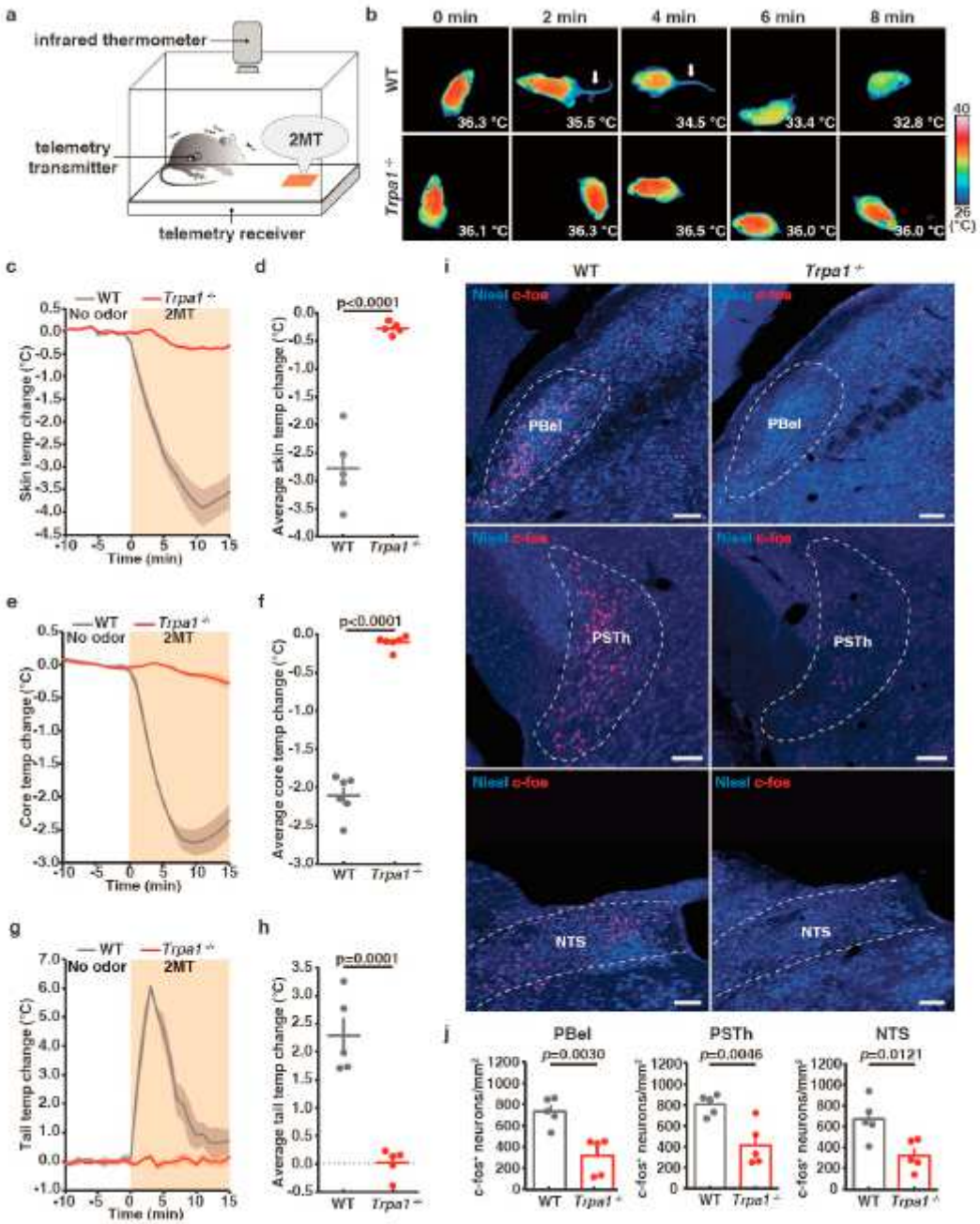

Figure 1

Innate fear odor 2MT induces hypothermia and tail temperature increase via Trpa1. a Schematic of 2MT-induced hypothermia assay in mice. b Time-lapsed thermal images showing tail and skin temperature changes in wild-type (upper) and Trpa1-/- (bottom) mice during 2MT treatment. c, e, g Tail (c), skin (e) and core (g) body temperature curves of wild-type and Trpa1-/- mice (n=5 or 6) before and during 2MT treatment. d, f, h Average tail (d), skin (f) and core (h) body temperature changes of wild-type and Trpa1-/- mice during 2MT treatment. i, Representative images showing 2MT-induced c-Fos expression in PBel, PSTh and NTS of wild-type and Trpa1-/- mice. j, Quantitative analysis of 2MT-evoked c-Fos expression in

PBel, PSTh and NTS in wild-type and Trpa1-/- mice (n=5). (c-h, j) Data are mean ± SEM; two-side Student's t test. Scale bars, 100 μm.

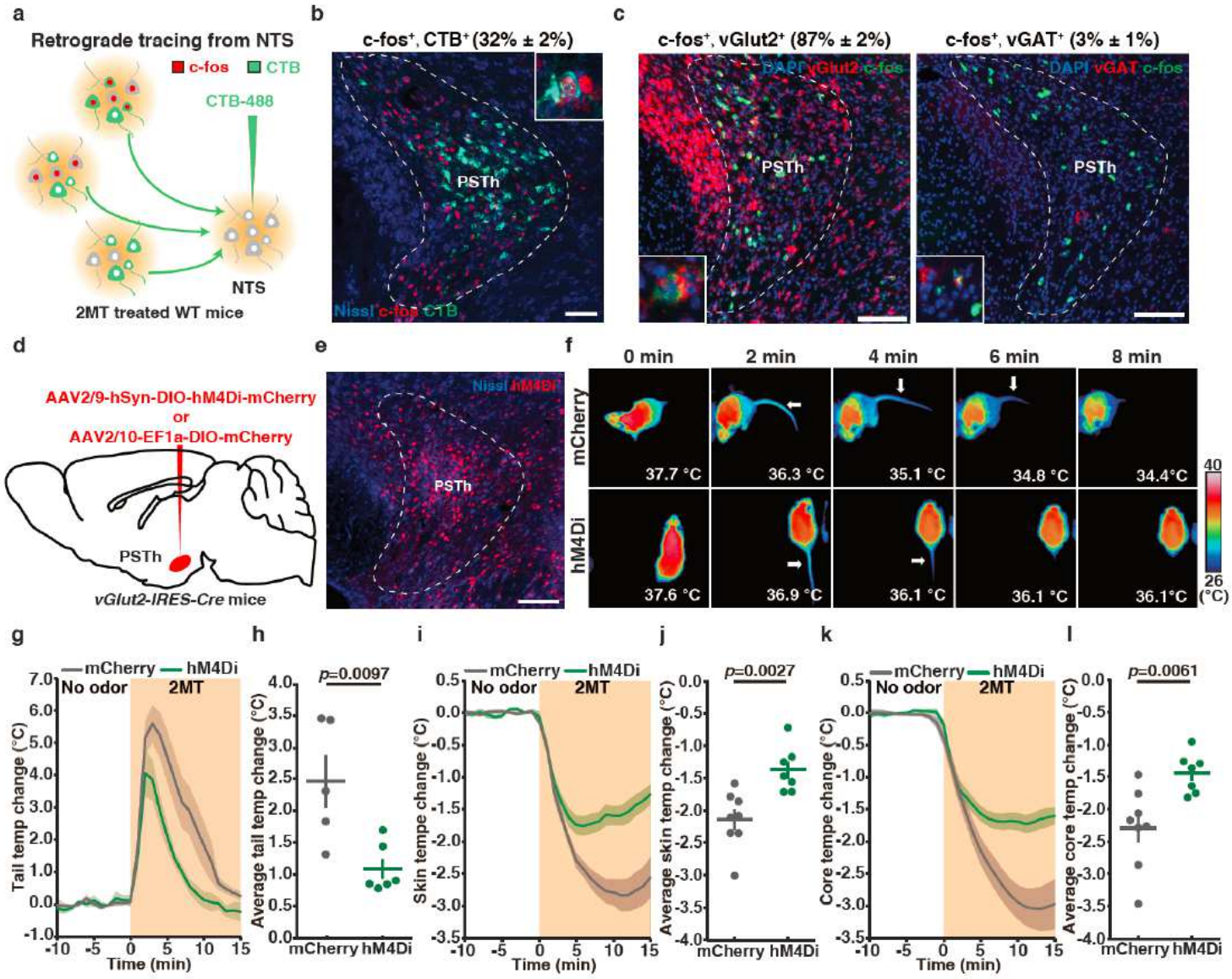

Figure 2

Inhibition of vGlut2+ PSTh neurons attenuates 2MT-evoked hypothermia and tail temperature increase. a Schematic of retrograde tracing from NTS neurons by CTB injection. b, Representative image showing double immunostaining of CTB and c-fos. The percentage of double positive neurons (CTB+, c-fos+/CTB+%) in PSTh is in parenthesis. c Representative images and quantitative analysis showing the percentage of c-fos+, vGlut2+ or c-fos+, vGAT+ double positive neurons among c-fos+ neurons in PSTh by two color in situ hybridization. d Schematic of chemogenetic inhibition experiment of vGlut2+ PSTh neurons in vGlut2-IRES-Cre mice. e Representative image of hMD4ilabeled vGlut2+ PSTh neurons. f Time-lapsed thermal images of mCherry-expressing mice and hM4Di-expressing mice during 2MT treatment following administration of C21. g, i, k Tail (g), skin (i) and core (k) temperature curves of mice with (hM4Di, n=7) or without (mCherry, n=8) inactivation of vGlut2+ PSTh neurons before and during 2MT treatment. h, j, l Average tail (h), skin (j) and core (l) temperature changes of mice with (hM4Di) or without

(mCherry) inactivation of vGlut2+ PSTh neurons during 2MT treatment. A few mice were not included in the analysis of tail temperature (e) because their tails were frequently obscured in the thermal images. (g-l) Data are mean ± SEM; two-side Student's t test. Scale bars, 100 μm.

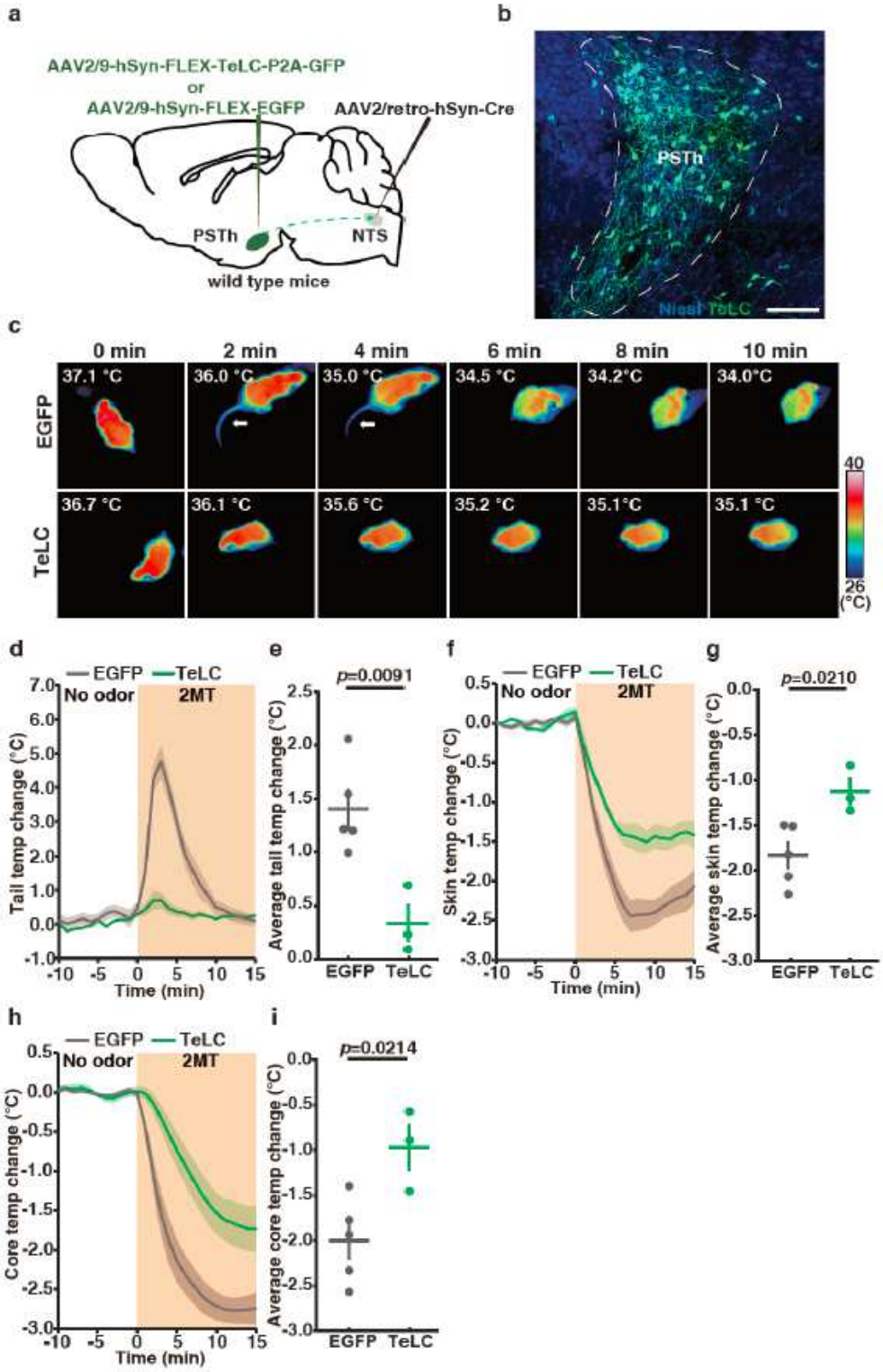

Figure 3

TeLC-mediated inactivation of NTS-projecting PSTh neurons diminishes 2MTevoked hypothermia and abrogates tail temperature increase. a Schematic of TeLC-mediated inactivation of PSTh neurons in wild-

type mice. b Representative image showing TeLC-GFP-labeled NTS-projecting PSTh neurons. c Time-lapsed thermal images of wild-type mice without (EGFP, up) or with (TeLC, bottom) inactivation of NTS-projecting PSTh neurons during 2MT treatment. d, f, h Tail (d), skin (f) and core (h) temperature curves of EYFPexpressing (n=5) and TeLC-expressing (n=3) mice before and during 2MT treatment. e, g, i Average tail (e), skin (g) and core (i) temperature changes of EGFP-expressing and TeLC-expressing mice during 2MT treatment. Two TeLC-expressing mice were not included in the analysis because of low virus transduction rate (Supplementary Fig. 3). (d-i) Data are mean ± SEM; two-side Student's t test. Scale bar, 100 μm.

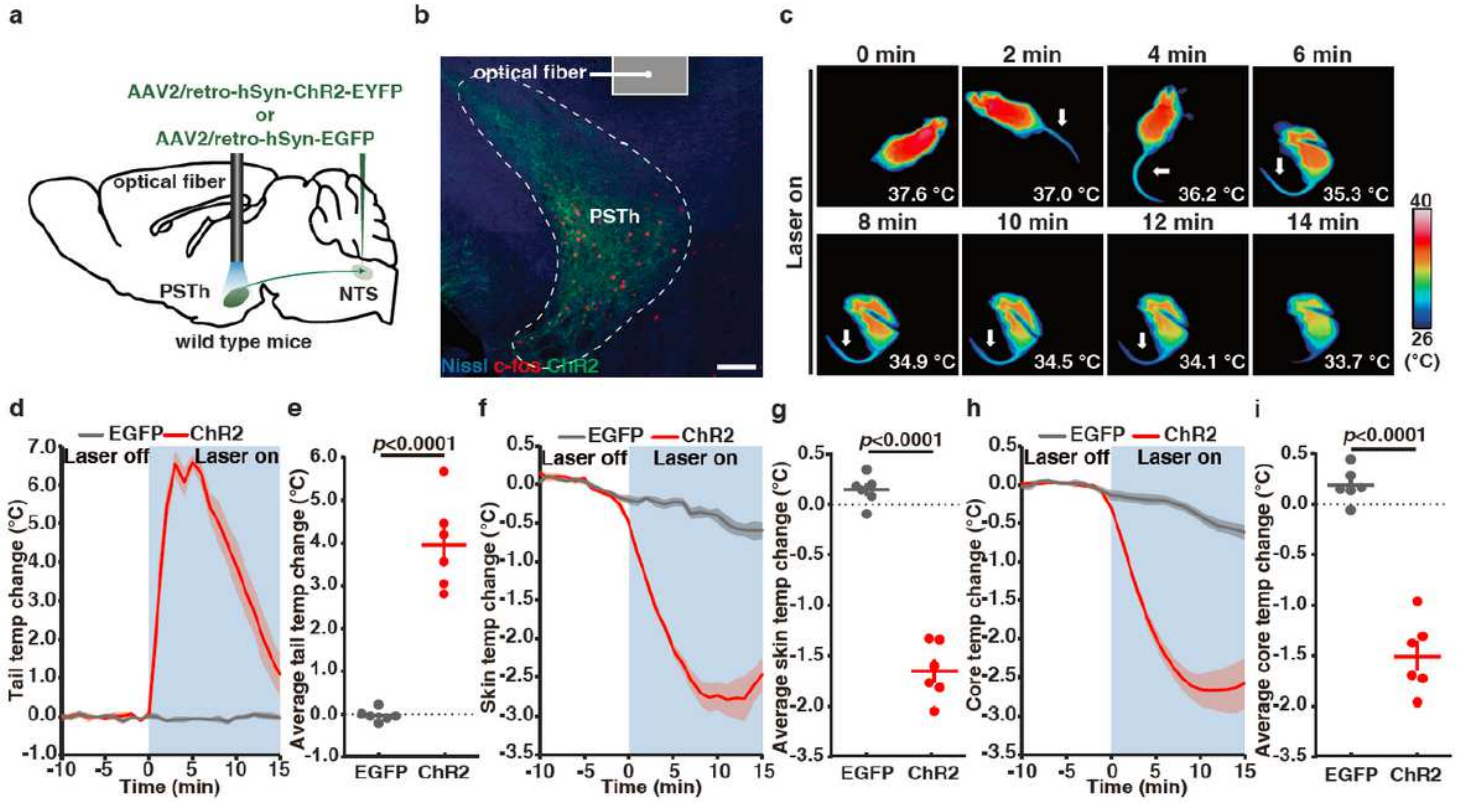

Figure 4

Activation of NTS-projecting PSTh neurons evokes hypothermia and tail temperature increase. a Schematic of optogenetic activation of the PSTh-NTS pathway in wild-type mice. b Representative image showing c-fos expression in ChR2-labeled PSTh neurons after photoactivation. c Timelapsed thermal images of ChR2-expressing mice during photoactivation of the NTS-projecting PSTh neurons. d, f, h Tail (d), skin (f) and core (h) temperature curves of EGFP-expressing (n=6) and ChR2-expressing mice (n=6) before and during photoactivation of the NTS-projecting PSTh neurons. e, g, i Average tail (e), skin (g) and core (i) temperature changes of EGFP-expressing and ChR2- expressing mice during photoactivation of NTS-projecting PSTh neurons. (d-i) Data are mean ± SEM; two-side Student's t test. Scale bar, 100 μm.

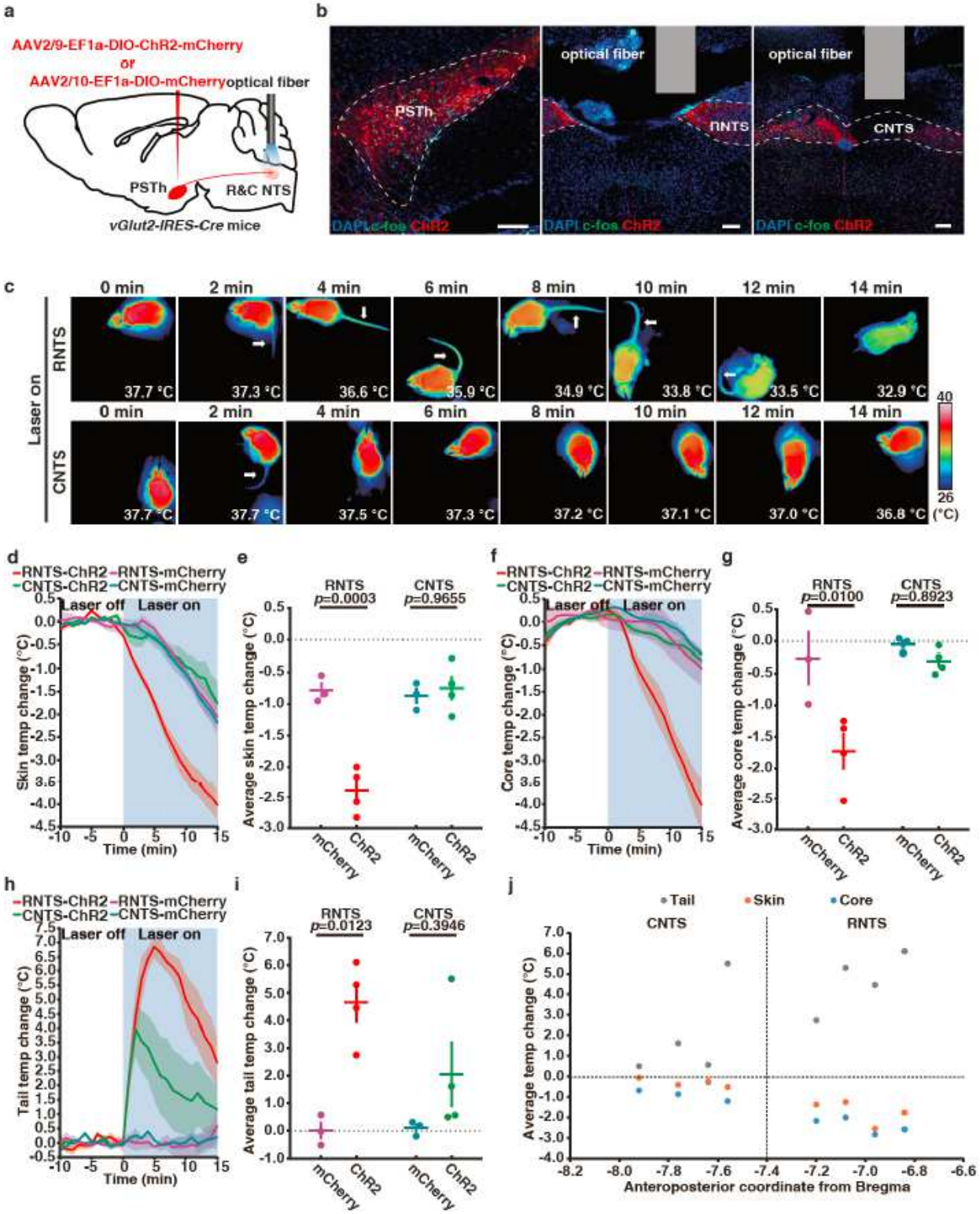

Figure 5

RNTS, but not CNTS, is the main target for hypothermia evoking PSTh neurons. a Schematic of optogenetic activation of the PSTh-NTS pathway in wild-type mice. b Representative images showing c-fos expression in ChR2-labeled PSTh neurons (left) and their axon terminals in RNTS (middle) and CNTS (right) in vGlut2-IRES-Cre mice after photoactivation. c Time-lapsed thermal images of ChR2-expressing mice during photoactivation of axon terminals of RNTS- or CNTS-projecting PSTh neurons. d, f, h skin (d),

core (f) and tail (h) temperature curves of mCherryexpressing (n=3) and ChR2-expressing mice (n=4) before and during photoactivation of axon terminals of RNTS- or CNTS-projecting PSTh neurons. e, g, i Average skin (e), core (g) and tail (i) temperature changes of mCherry-expressing and ChR2-expressing mice during photoactivation of axon terminals of RNTS- or CNTS-projecting PSTh neurons. j Correlative analysis between the photoactivation-induced average tail, skin and core temperature changes in ChR2-expressing mice and the anteroposterior coordinates of the optical fiber implant sites. (d-i) Data are mean ± SEM; two way ANOVA analysis followed by Tukey's multiple comparisons test. Scale bars, 100 μm.

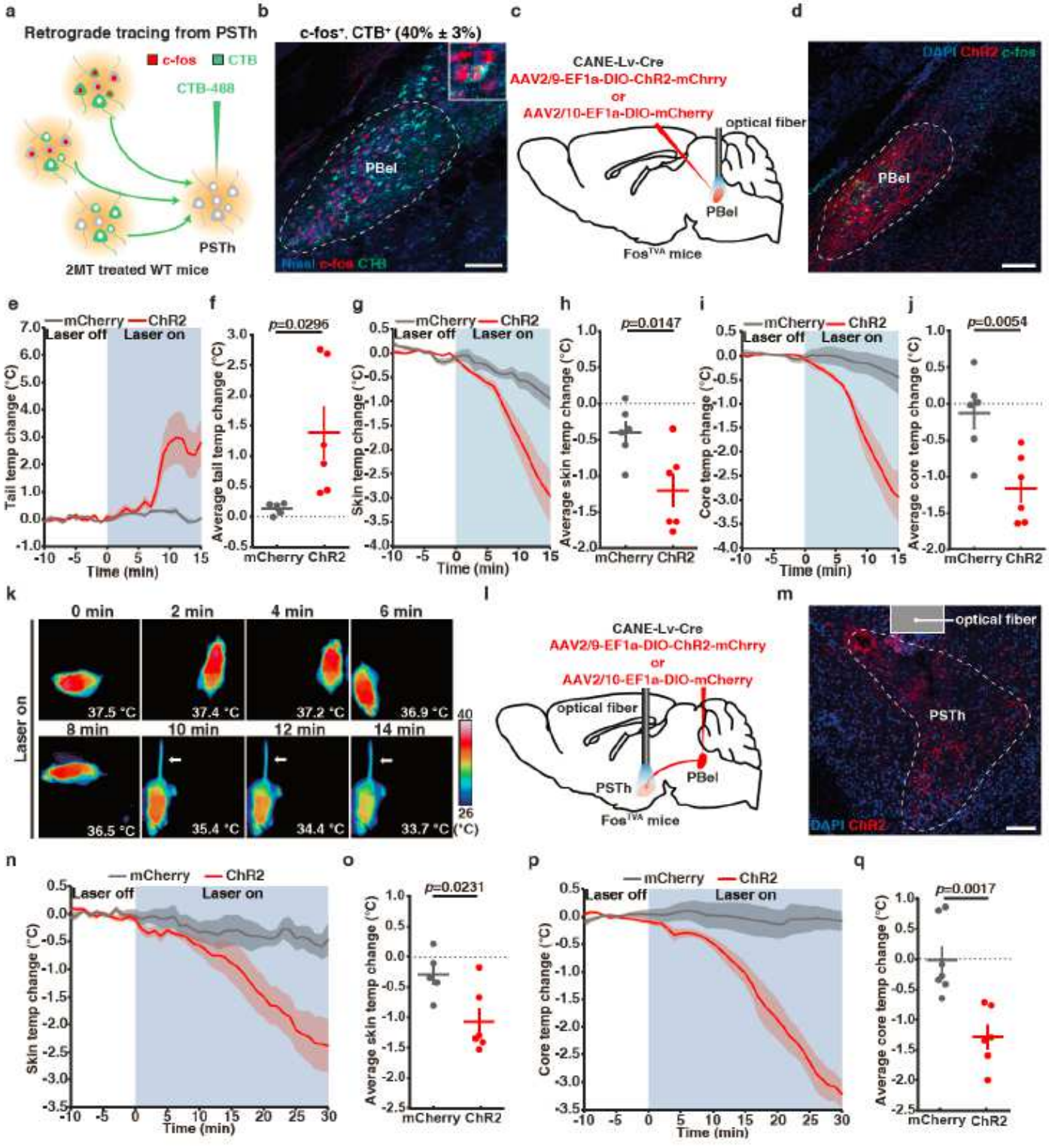

Figure 6

Activation of 2MT-activated PBel neurons and their axonal inputs to PSTh evokes hypothermia. a Schematic of retrograde tracing from PSTh neurons by CTB. b Representative images showing double immunostaining of CTB and c-fos. The percentage of c-fos+, CTB+ neurons among CTB+ neurons in PBel is shown in parenthesis. c Schematic of selective opto-stimulation of the cell bodies of 2MT-activated PBel neurons labeled by CANE in FosTVA mice. d. Representative images showing c-fos expression in the ChR2-labeled PBel neurons following photoactivation. e, g, i Tail (e), skin (g) and core (i) temperature curves of mCherry-expressing (n=5 or 7) and ChR2-expressing (n=6) FosTVA mice before and during blue light stimulation of 2MT-activated PBel neurons. f, h, i Average tail (f), skin (h) and core (j) temperature changes of mCherry-expressing and ChR2-expressing FosTVA mice during opto-stimulation of 2MT-activated PBel neurons. k Time-lapsed thermal images of ChR2-expressing FosTVA mice during photoactivation of 2MT-activated PBel neurons. l Schematic of selective opto-stimulation of the axon terminals of 2MT-activated PBel neurons in PSTh in FosTVA mice. m Representative images showing the ChR2-labeled axon terminals from 2MT-activated PBel neurons in PSTh. n, p Skin (n) and core (p) temperature curves of mCherry-expressing (n=5 or 7) and ChR2-expressing (n=6) FosTVA mice before and during blue light stimulation of axon terminals in PSTh. o, q Average skin (o) and core (q) temperature changes of mCherry-expressing and ChR2- expressing FosTVA mice during blue light stimulation of axon terminals in PSTh. (e-j, n-q) Data are mean ± SEM; two-side Student’s t test. Scale bars, 100 μm

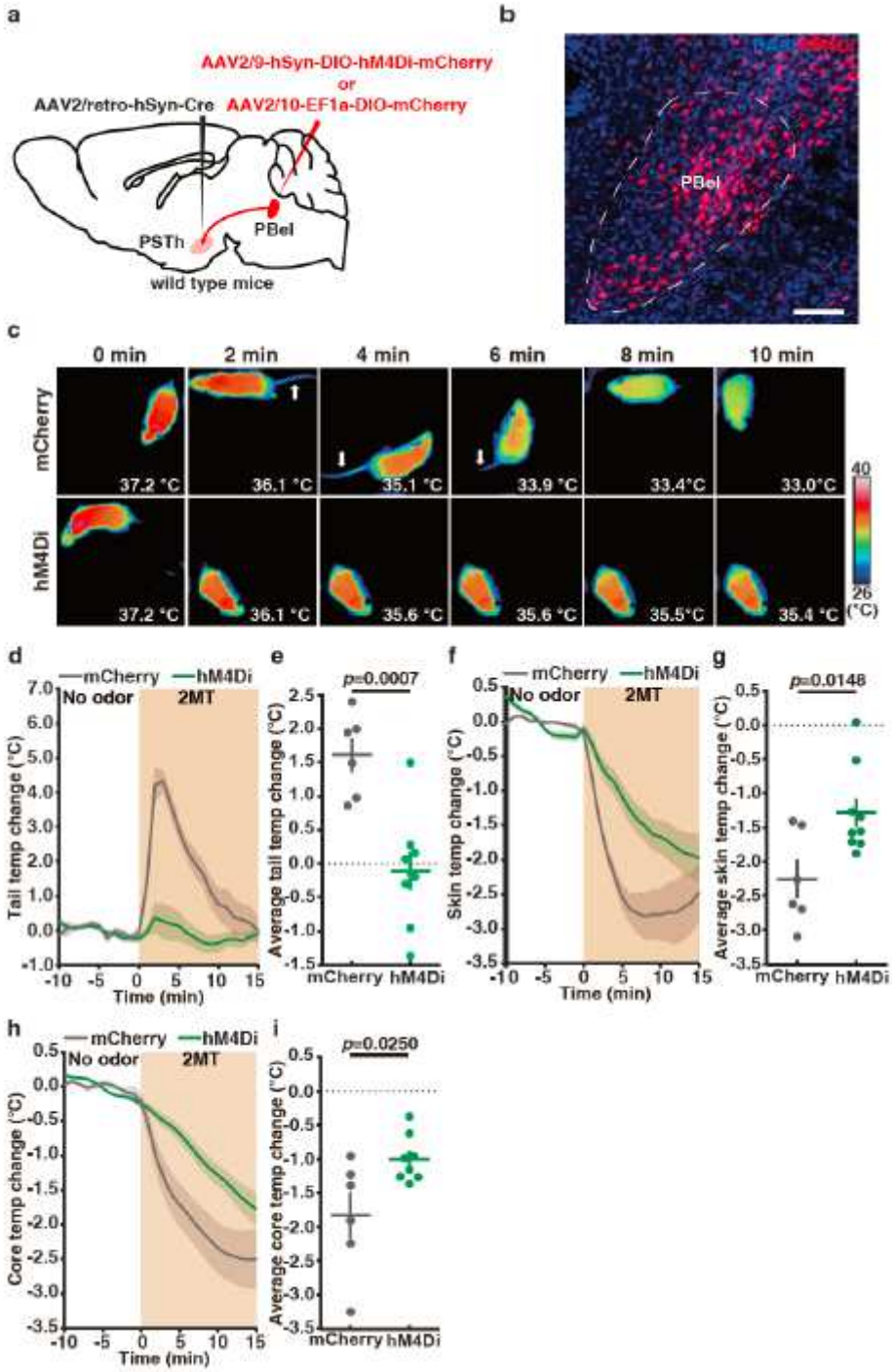

Figure 7

Inhibition of PSTh-projecting PBel neurons diminishes 2MT-evoked hypothermia and tail temperature increase. a Schematic of chemogenetic inhibition PSTh-projecting PBel neurons. b Representative image of hMD4i-labeled PSTh-projecting PBel neurons. c Time-lapsed thermal images of mCherryexpressing mice and hM4Di-expressing mice during 2MT treatment following administration of C21. d, f, h Tail (d), skin (f) and core (h) temperature curves of mice with (hM4Di, n=8 or 9) or without (mCherry, n=6) inactivation of PSTh-projecting PBel neurons before and during 2MT treatment. e, g, i Average tail (e), skin (g) and core (i) temperature changes of mice with (hM4Di) or without (mCherry) inactivation of

PSTh-projecting PBel neurons during 2MT treatment. (d-i) Data are mean ± SEM; two-side Student's t test. Scale bar, 100 μm.

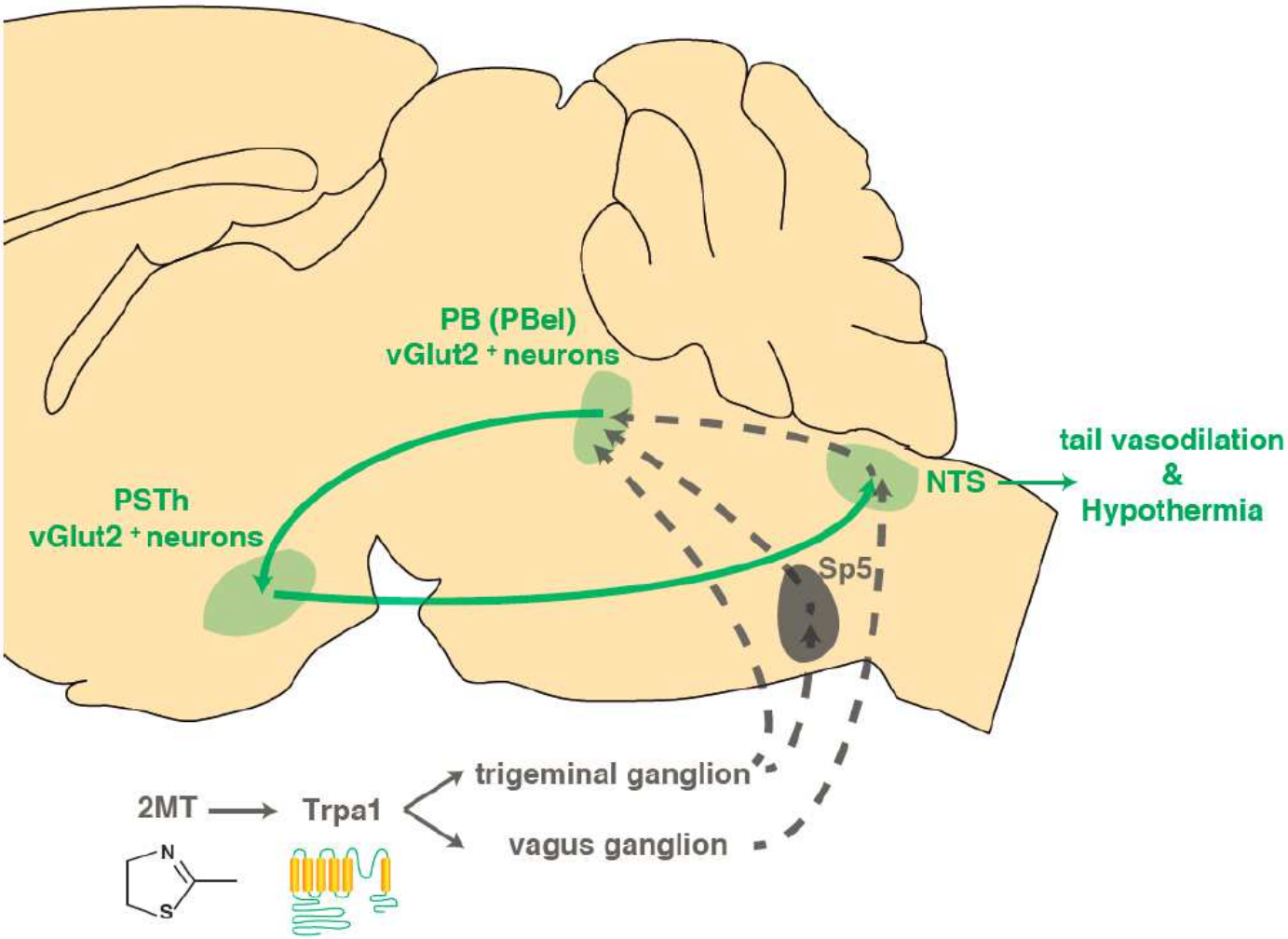

Figure 8

Neural pathways for 2MT-evoked hypothermia.